Accelerating Invasions and the Asymptotics of Fat-tailed Dispersal

Benjamin R. Liu[a], Mark Kot[a]

[a]*Department of Applied Mathematics, University of Washington, Box 353925, Seattle, WA 98195-3925*

Abstract

Integrodifference equations (IDEs) are used in ecology to model the growth and spatial spread of populations. With IDEs, dispersal is specified with a probability density function, called the dispersal kernel, and the shape of the kernel influences how rapidly invasions progress. In this paper, we apply tail additivity, a property of regularly varying probability densities, to model invasions with fat-tailed (power-law decay) dispersal in one dimension. We show that fat-tailed invasions progress geometrically fast, with the rate of spread depending on the degree of fatness of the tails. Our analyses apply to populations with no Allee effect as well as weak Allee effects, and we conduct simulations to show that fat-tailed invasions with weak Allee effects produce accelerating invasions. We analyze point-release and front-release invasions, corresponding to newly-established and well-established populations, and find that front-release invasions gain a permanent speed-up over point-release invasions, invading at a faster geometric rate that persists for all time. Since accelerating invasions are qualitatively different than constant-speed invasions, we also discuss how measures of invasion must be modified and reconsidered when invasions accelerate.

Keywords: Allee effect, biological invasions, heavy tails, integrodifference equations, regular variation

Highlights:

- Regular variation is a powerful tool for analyzing fat-tailed (power-law decay) invasions.
- Fat-tailed invasions advance at geometric rates governed by the net reproductive rate and the degree of fatness of the tails of the dispersal kernel.
- Analyses apply to populations with no Allee effect and weak Allee effects.
- Different initial conditions can result in permanent and transient changes in the rate of geometric spread of the invasion.
- Measuring fat-tailed, accelerating invasions requires different approaches than measuring thin-tailed, constant-speed invasions.

1. Introduction

Classical models for biological invasions, such as Fisher's (1937) reaction-diffusion model, implicitly assume Gaussian dispersal (Lewis, 1997; Lewis et al., 2016). Many recent researchers have, in contrast, focused on leptokurtic, heavy-tailed, and long-distance dispersal (Bullock and Clarke, 2000; Cain et al., 2000; Nathan et al., 2003; Nathan, 2005; Klein et al., 2006; Nathan et al., 2008; Mundt et al., 2009). Leptokurtic and heavy-tailed dispersal assign a much larger probability to traveling long distances than does Gaussian dispersal.

Integrodifference equations (IDEs) provide one way of accounting for long-distance dispersal. IDEs are discrete-time, continuous-space population models that assume discrete, non-overlapping generations and distinct growth and dispersal stages (Kot et al., 2012). IDEs are more flexible than reaction-diffusion models in that they specify dispersal using a dispersal kernel, a probability density function for the displacement of the propagules (Kot et al., 1996; Nathan et al., 2012).

One of the key properties of a dispersal kernel is whether it is thin- or heavy-tailed. Thin-tailed kernels possess moment generating functions, while heavy-tailed kernels do not. With thin-tailed kernels, IDEs behave like reaction-diffusion equations: they quickly produce traveling waves that advance with constant invasion speeds (Weinberger, 1982; Kot, 1992; but see Sullivan et al., 2017 for an important counterexample). Gaussian kernels generate invasion speeds that exactly match those of reaction-diffusion systems, while leptokurtic distributions produce invasions that move faster but with finite speeds. Existing work (Lewis et al., 2006; Kot and Neubert, 2008) has characterized the invasion speed of thin-tailed invasions in terms of moment generating functions.

Invasion with heavy-tailed dispersal is more poorly understood. Methods based on moment generating functions cannot be extended to heavy-tailed kernels since these kernels lack moment generating functions. Kot et al. (1996) performed heuristic analyses and conducted simulations for point-release invasions with kernels with moments all finite. They argued that populations with heavy-tailed dispersal have spatial distributions with tails that mirror

those of the dispersal kernel itself. They concluded that heavy-tailed invasions accelerate without bound, achieving infinite invasion speeds; however, their arguments were limited to point-release invasions and could not be extended with generality to kernels with heavier tails.

Accelerating invasions are qualitatively different than those that progress at a constant speed. Beyond simply needing new analytic techniques for finding the rate of invasion, underlying assumptions about the nature of these invasions such as how we measure and define spatial extent and the rate of change of that extent need to be modified when dealing with accelerating invasions.

In this paper we use *regularly varying densities* to model fat-tailed invasions in one dimension. Regular variation can be thought of as a generalization of the behavior of power-law functions. We adapt the *tail additivity* properties of regularly varying probability densities to model invasions from newly-established and well-established populations. Tail additivity is an asymptotic property that allows the tails of convolved functions to be approximated in terms of the tails of the original functions. We show how these properties enable powerful analyses. We find the rate of spread for invasions under the linear and nonlinear model, for populations with and without (weak) Allee effects.

This paper has 9 sections. In *Model*, we introduce the nonlinear, one-dimensional integrodifference equation that we study, and its linearization. We discuss the two components of the model, the dispersal kernel $k(x)$ and the growth function $f(n)$. We review the concepts of weak and strong Allee effects, and then summarize how these effects alter invasions. We also introduce the two types of initial conditions, point-release and front-release, that we will analyze. The section *Dispersal kernels and tails* covers classifications of tail heaviness, relevant definitions from probability, and introduces regularly varying densities and the tail additivity properties that are central to our analyses.

In *Point-release initial conditions*, we focus on invasions beginning with small, localized source populations. We use tail additivity to analyze the linear and nonlinear models and derive invasion rates for fat-tailed kernels. Our analyses apply to populations that grow with no Allee effect or weak Allee effects, and, in *Weak Allee effects*, we demonstrate this with numerical simulations and show how fat-tailed invasions change as the strength of the Allee effect changes. In contrast to newly emerging populations, we also have populations that already occupy large territories. We analyze invasions by well-establish populations in the section *Front-release initial conditions*.

Our analyses of point- and front-release invasions lead us to conclude that they invade at different rates. We discuss this and show examples in *Invasion rates and initial conditions*, and we perform simulations with a type of initial condition that is intermediate to point- and front-release invasions. In *Accelerating waves*, we discuss the differences between constant-speed and accelerating invasions and how these differences require us to adapt our strategies for measurement and analysis. In *Discussion*, we interpret and discuss the implications of our results and talk about some directions for future work.

2. Model

Consider a population with discrete non-overlapping generations and distinct growth and dispersal stages. Let $n_t(x)$ be the (one-dimensional) density of this population at time t. We will model the density of this population in the next generation with the integrodifference equation (IDE)

$$n_{t+1}(x) = \int_{-\infty}^{\infty} k(x,y) f\left(n_t(y)\right) \mathrm{d}y. \tag{2.1}$$

Like the population, this model can be understood in terms of distinct stages. The *growth function* $f(n)$ describes the recruitment of the next generation during the sedentary stage, as a function of the distribution of the current population. The *dispersal kernel* $k(x,y)$ is a probability density function that gives the probability that offspring from location y settle in location x. The integral sums up dispersal from all possible sources.

If the dispersal kernel $k(x,y)$ only depends on the difference $x-y$, dispersal is homogeneous and the IDE reduces to a convolution,

$$\begin{aligned} n_{t+1}(x) &= \int_{-\infty}^{\infty} k(x-y) f\left(n_t(y)\right) \mathrm{d}y \\ &= \left[k * f(n_t)\right](x). \end{aligned} \tag{2.2}$$

We will focus on convolution-type IDEs throughout this paper.

In addition to *nonlinear* IDE (2.2) we also concern ourselves with its *linearization*,

$$\begin{aligned} n_{t+1}(x) &= R_0 \int_{-\infty}^{\infty} k(x-y) n_t(y) \mathrm{d}y \\ &= R_0 \cdot (k * n_t)(x). \end{aligned} \tag{2.3}$$

This IDE is obtained by linearizing the growth function $f(n)$ about zero, replacing $f(n)$ with $R_0 n$, since

$$f(n) \sim f'(0) n = R_0 n \quad \text{as} \quad n \to 0. \tag{2.4}$$

We linearize to study invasions where unoccupied territory is colonized. At these low densities where $n \approx 0$, the linear model has dynamics very similar to those of the nonlinear model. The linear model is, however, easier to analyze.

As we will see, there are three main components that affect how a population governed by these models will spread: the growth function, the dispersal kernel, and the initial distribution of the population.

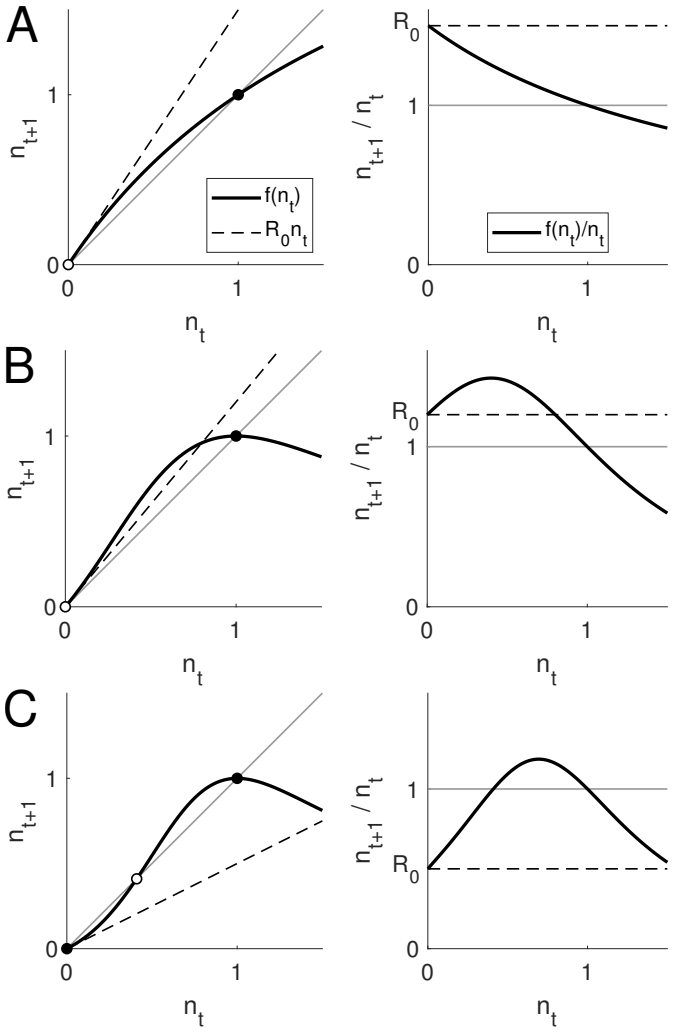

Figure 1: Example growth functions. Left plots show the growth function $n_{t+1} = f(n_t)$ (black curves) with the identity line $n_{t+1} = n_t$ (solid gray) and the line $n_{t+1} = R_0 n_t$ (dashed black). Circles indicate equilibria: filled circles are stable, and empty circles are unstable. Right plots show the per capita recruitment, n_{t+1}/n_t, which more clearly show Allee effects. **(A)** Growth with no Allee effect. Such growth functions have no depensatory effects. The function has maximum slope R_0 at $n_t = 0$ and the per-capita recruitment never exceeds R_0. **(B)** Growth function with a weak Allee effect. Such growth is characterized by a net reproductive rate $R_0 > 1$ and the per-capita recruitment exceeding the value of R_0 at some point $n_t > 0$. In other words, the graph of $n_{t+1} = f(n_t)$ rises above $n_{t+1} = R_0 n_t$. **(C)** Growth function with a strong Allee effect. The growth function lies below the line $n_{t+1} = n_t$ for small values of n_t. This means $R_0 < 1$.

2.1. Nonlinear growth and Allee effects

The growth function $f(n)$ describes the survival and reproduction, or recruitment, during the sedentary stage. Without dispersal, the population density at time $t+1$ is given by

$$n_{t+1} = f(n_t). \tag{2.5}$$

Typically both zero and the carrying capacity are fixed points of the growth function. Fixed points are points where $n_{t+1} = n_t = n^*$ or $f(n^*) = n^*$ and are also known as equilibria. If we rescale the carrying capacity to be one, this means that $f(0) = 0$ and $f(1) = 1$. Other fixed points can also occur, as in the case of bistability where an unstable equilibrium lies between stable equilibria at zero and one. We will, however, focus exclusively on monostable growth functions, where $n^* = 1$ is a stable and $n^* = 0$ is an unstable equilibrium. Examples of growth functions and their equilibria can be seen in Figure 1. In this figure, equilibria are indicated by filled (stable) and hollow (unstable) circles.

In practice, the growth function is typically smooth or at least continuous. Discontinuous growth functions are sometimes used, especially in mathematical studies where simple forms are required to make analysis tractable (Kot et al., 1996; Wang et al., 2002; Lewis et al., 2016) or when the effect of changing specific aspects of the growth function need to be measured in isolation. We always assume that the derivative exists at $n = 0$, and we denote $R_0 = f'(0)$ as the net reproductive rate. The value R_0 determines how a population grows at low densities and is important in determining its rate of invasion.

When the growth function satisfies $f(n) \leq R_0 n$, it is said to have *no Allee effect*, and the rate of invasion is completely determined by the form of dispersal $k(x)$ and the value R_0. When this condition is violated, an Allee effect is present, meaning that the per capita recruitment $f(n_t)/n_t$ decreases, for decreasing n_t, near the origin. Allee effects can be weak or strong (Wang et al., 2002) and are distinguished by whether $f(n)$ is greater than or less than n near the origin or, equivalently, whether $R_0 > 1$ or $R_0 < 1$. If $R_0 > 1$, then an arbitrarily small population persists and grows. If, in contrast, $R_0 < 1$, too few offspring replace their parents and the population perishes. Figure 1 shows examples of growth functions with no Allee effect as well as with weak and strong Allee effects.

Allee effects are especially important when considering and extrapolating from the behavior of a linear model such as (2.3). It has long been conjectured that the invasion speed of a nonlinear model will match that of its linearization under two conditions (van den Bosch et al., 1990):

> (i) The average rate of reproduction of an individual experiencing throughout its life an environment 'occupied' by a certain (possibly varying) population is always smaller than the rate of reproduction in a 'virgin' environment (i.e. in particular there are no Allee-like effects), and that
>
> (ii) The influence of an individual on the environment very far from its (present) position is negligible.

Mollison (1991) clarifies that (ii) relates not to long-distance dispersal, but rather to nonlocalities in the growth of the population: there should be no long-distance density dependence. This is not an issue in our model formulation, where the population growth $f(n(x))$ depends only on the density at that same point.

2.2. Initial conditions

The population density $n_0(x)$ at the starting time $t = 0$ is called the *initial condition*. Any initial population density can be considered, but we will focus on two types of conditions.

Point-release initial conditions specify that the initial population is released in a small area, approximated by a point. In practice this is handled in a number of ways. If N_0 is the initial total population, then one way is to choose a width L on which to set the population density at a constant level, which approximates the initial distribution as a patch of concentrated population,

$$n_0(x) = \begin{cases} \dfrac{N_0}{L} & -L/2 \le x \le L/2 \\ 0 & \text{otherwise.} \end{cases} \tag{2.6}$$

Decreasing the width L narrows the patch and concentrates the population. Another common approach is to specify the initial condition as a scaled Gaussian distribution,

$$n_0(x) = \frac{N_0}{\sqrt{2\pi\sigma^2}} e^{-x^2/(2\sigma^2)}. \tag{2.7}$$

As in the case of the finite patch, the standard deviation σ of the Gaussian can be made small to reduce its width and concentrate the population. For analysis based on the linear model, where one can mathematically switch the order of growth and integration, the Dirac delta function is commonly used, and can be thought of as the limiting case of the Gaussian where $\sigma \to 0$; for more information, see the derivation of a formal solution under the linear model in section *Point-release initial conditions*.

Front-release initial conditions are those where a front or boundary exists, to one side of which is populated territory and to the other uncolonized territory. In contrast with a newly emerging or developing point-release invasion, a front-like invasion has a well-established population behind the front.

We would like to make precise the notion of a well-established population that is invading new territory. We define a one-dimensional spatial population density $n(x)$ to be *front-like* if: (1) $n(x)$ is non-decreasing, (2) $n(x)$ goes to zero as x approaches $-\infty$, and (3) $n(x)$ goes to the population carrying capacity as x approaches $+\infty$.

Alternative definitions of front-like population density profiles are possible. Alfaro and Coville (2017) define "front like initial data" $u_0(x)$ as having (i) $0 \le u_0(x) < 1$, (ii) $\liminf_{x\to-\infty} u_0(x) > 0$, and (iii) $u_0 \equiv 0$ for some $a \le x < \infty$. This condition imposes a stricter condition on the virgin territory (that the population density truly vanishes rather than decays to zero) and a weaker condition on the colonized territory (that the population density stays above a nonzero value, rather than approaching the carrying capacity). Our definition suits our analyses where we cast population densities as cumulative distribution functions.

3. Dispersal kernels and tails

In this section we discuss aspects of probability theory relevant to dispersal in ecology. We begin with a review of terminology from the probability literature. This builds to a discussion of tail heaviness, including some terms that are often treated differently in ecology and probability. We introduce regularly varying densities and the tail additivity properties of their convolutions that form the basis for our analyses. We conclude with examples of fat-tailed kernels that we use in numerical simulations throughout the paper.

3.1. Probability review

Dispersal can be thought of as as a random process, with X the random displacement (in one dimension) and $k(x)$ the probability density function for this displacement. In ecology, this probability density function is often called the dispersal kernel.

In addition to the probability density function, every distribution can be characterized by a *cumulative distribution function* or cdf that encodes the probability of X being any value up to a specified value x,

$$K(x) = \Pr\{X \le x\}. \tag{3.1}$$

A cdf is related to its pdf by the derivative: $K'(x) = k(x)$.

The term "dispersal kernel" is somewhat vague, because some use it to describe the probability distribution of dispersal distances. Nathan proposes calling this the *dispersal distance kernel* (Nathan et al., 2012). Under Nathan's conventions, we will be working exclusively with *dispersal location kernels* in one dimension, and we will denote these kernels as $k(x)$ for the pdf and $K(x)$ for the cdf.

In this paper we focus on distributions that are *symmetric*, so $k(x) = k(-x)$ for all real x. This simplifies things a great deal and allows us to be relaxed about subtleties such as heavy *left* or *right* tails with differing rates of invasion to the left or right; our dispersal kernels are simply heavy-tailed, meaning both tails are heavy. Asymmetric kernels can lead to unequal rates of leftward and rightward spread and are sometimes introduced by advective forces such as the current in a river or by the movement of a habitat in climate change models (Lutscher and Seo, 2011; Vasilyeva and Lutscher, 2012; Phillips and Kot, 2015).

The expected value $E[X]$ of X is its mean value, also called the *first raw moment*, and is calculated as

$$E[X] = \int_{-\infty}^{\infty} xk(x)\mathrm{d}x. \tag{3.2}$$

This integral does not converge for some kernels with very heavy tails, such as the Cauchy distribution; this is not a

fault of the definition of the mean, but rather a statement about the extraordinarily heavy tails of these distributions.

Other expectations of functions of X can also be computed. For instance, the n-th raw moment of X is given by

$$\mu'_n = E[X^n] = \int_{-\infty}^{\infty} x^n k(x) \mathrm{d}x, \tag{3.3}$$

The raw moments may all be finite values, or some may *diverge* or not exist, when the expectation integral fails to converge, as in the case of the mean of the Cauchy distribution.

The moment generating function (mgf) of a distribution is a function defined as an expectation:

$$M(s) = E\left[e^{sX}\right] = \int_{-\infty}^{\infty} e^{sx} k(x) \mathrm{d}x. \tag{3.4}$$

The mgf may be defined on the whole real line or only part of it. The value $M(0) = 1$ is always defined, but $M(s)$ may be undefined for all nonzero values of s. When this is the case, we say that the mgf does not exist or that the distribution lacks a mgf. The moment generating function is so-named because if the mgf exists, then its Taylor series,

$$M(s) = 1 + \mu'_1 s + \frac{\mu'_2}{2!} s^2 + \frac{\mu'_3}{3!} s^3 + \cdots, \tag{3.5}$$

encodes the raw moments of the distribution.

3.2. Degrees of heaviness and types of tails

Various descriptions of kernel shape and tail heaviness are used in probability and ecology. Classical approaches such as reaction-diffusion equations model dispersal by diffusion, which implicitly assumes Gaussian dispersal. Excess kurtosis, a measure of broadness of dispersal in relation to the Gaussian distribution, was a natural metric for studies that departed from Gaussian dispersal. Today it is more common to speak of "heavy-tailed" or "fat-tailed" distributions. Long-distance dispersal events are said to occur due to heavy-tailed dispersal, and high excess kurtosis is entailed.

The kurtosis of a random variable X is defined as the expectation

$$\kappa = E\left[\left(\frac{X-\mu}{\sigma}\right)^4\right], \tag{3.6}$$

where $\mu = E[X]$ is the mean and $\sigma^2 = E[(X-\mu)^2]$ the variance. The kurtosis of the standard normal (Gaussian) distribution is 3, and so the kurtosis of other distributions when compared to the Gaussian is reported as the *excess kurtosis*, $\kappa - 3$. Distributions with zero excess kurtosis are called mesokurtic, those with negative excess kurtosis are platykurtic, and positive excess kurtosis are termed leptokurtic. Kurtosis is sometimes used in descriptions of tail heaviness. Leptokurtic distributions are those whose extreme values are "more probable than normal" (Cooke et al., 2014). In ecology, dispersal is most commonly leptokurtic (Bateman, 1950; Nathan et al., 2012).

Thin-tailed or *light-tailed* distributions possess moment generating functions. For continuous random variables, this means that there exists some $s > 0$ such that

$$E\left[e^{sX}\right] = \int_{-\infty}^{\infty} e^{sx} f_X(x) \mathrm{d}x < \infty. \tag{3.7}$$

Thin-tailed distributions are sometimes called *exponentially-bounded* in ecology. This means that there exists some $s > 0$ and x^* such that $k(x) < \exp(-sx)$ for all $x > x^*$. When a distribution is exponentially bounded, the integral (3.7) must converge, and so the moment generating function must exist, although the converse is not true: there exist some exotic probability densities that are not exponentially-bounded, yet which do possess moment generating functions.

Two common thin-tailed distributions are the Gaussian or normal distribution,

$$k(x) = \frac{1}{\sqrt{2\pi\sigma^2}} e^{-x^2/(2\sigma^2)}, \tag{3.8}$$

and the Laplace (double-exponential) distribution,

$$k(x) = \frac{1}{2b} e^{-|x|/b}, \tag{3.9}$$

both shown here with zero mean. These distributions can be seen in Figure 2, plotted in a variety of scales. The thin tails of these distributions can be visually identified by the fact that they decay as rapidly or faster than a diagonal line in a linear-log plot, which means they are exponentially-bounded.

Heavy-tailed distributions lack moment generating functions. The set of heavy-tailed distributions is therefore the complement (for symmetric kernels) of thin-tailed distributions. Re-examining the Taylor series representation of the moment generating function (3.5), one way by which the mgf may fail to exist is that some of the moments are divergent (infinite). Another possibility is that all of the moments exist and are finite but taken together the infinite series fails to converge. Distributions may be heavy-tailed for either of these reasons.

Heavy-tailed distributions do not have exponentially-bounded tails. In fact, most commonly used heavy-tailed distributions will eventually dominate any decaying exponential. That is, for any decaying exponential function, e^{-sx} for any value of $s > 0$, then at some point x^*, $k(x) > e^{-sx}$ for all $x > x^*$. This means that no matter how slowly the exponential decays, eventually $k(x)$ will exceed it.

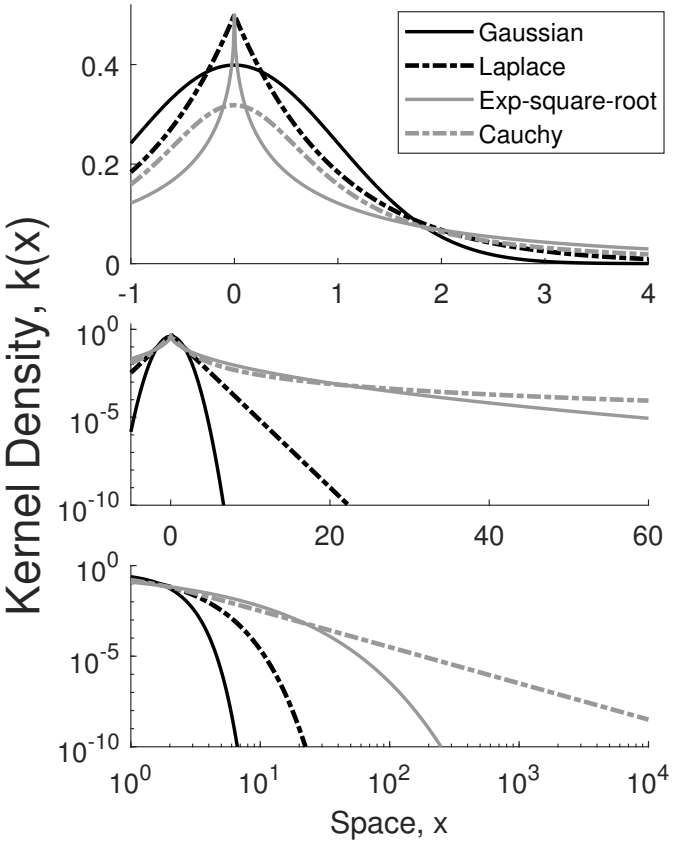

Figure 2: Tails of various probability density functions. Gaussian, Laplace, Cauchy, and exponential square-root distributions, equations (3.8), (3.9), (3.10), and (3.12), at a variety of scales. The first two distributions are thin-tailed, the third distribution is fat-tailed, and the fourth distribution is heavy-tailed but not fat-tailed. **(Top)** The kernels plotted on a linear-linear scale, showing the shape of the kernels near the origin. **(Middle)** A linear-log scale plot, where the relative magnitudes of the tails are more clearly visible. The tails of the Laplace density decay exponentially, and so appear as straight lines. The heavier-tailed exponential square-root and Cauchy kernels flatten in linear-log scale. **(Bottom)** The kernels on a log-log scale. Here the fat-tailed Cauchy kernel has tails that tend toward straight lines.

A classic example of a heavy-tailed kernel is the Cauchy distribution,

$$k(x) = \frac{b}{\pi(b^2 + x^2)}. \tag{3.10}$$

Its heavy-tailedness can be seen by examining the limit of $k(x)/\exp(-sx)$,

$$\lim_{x\to\infty} \frac{be^{sx}}{\pi(b^2 + x^2)} = \infty, \tag{3.11}$$

which is evident from the fact that any growing exponential function will grow faster than any polynomial. Since the limit $k(x)/\exp(-sx)$ is infinite, the magnitude of $k(x)$ eventually dominates the decaying exponential (for any value of s). Another heavy-tailed kernel is the exponential square-root,

$$k(x) = \frac{1}{b} e^{-2\sqrt{|x|/b}}. \tag{3.12}$$

Again examining the limit of $k(x)/\exp(-sx)$, we find

$$\lim_{x\to\infty} \frac{1}{b} e^{sx - 2\sqrt{x/b}} = \infty, \tag{3.13}$$

which can be seen by observing that any linear function will grow faster than any square-root function, again showing that $k(x)$ eventually dominates any decaying exponential. These distributions are presented in Figure 2 alongside two thin-tailed ones. Their heavy tails can be seen clearly on a linear-log plot where their tails flatten, such that they will eventually dominate any diagonal line.

Fat-tailed distributions are among the heaviest of heavy-tailed kernels. They decay asymptotically as power laws, so that there exists some $\alpha > 1$ and $c > 0$ such that

$$k(x) \sim cx^{-\alpha}, \qquad x \to \infty. \tag{3.14}$$

Here α is the *degree* or *order* of tail fatness that specifies the order of power-law decay of the tail and c is a normalization constant that causes $k(x)$ to integrate to one. The notation $k(x) \sim g(x)$ reads as $k(x)$ *is asymptotically equivalent to* $g(x)$, and means that

$$\lim_{x\to\infty} \frac{k(x)}{g(x)} = 1. \tag{3.15}$$

An example of a fat-tailed kernel is Cauchy kernel (3.10), which can be verified as fat-tailed since it is a rational function,

$$k(x) = \frac{b}{\pi(b^2 + x^2)} \sim \frac{b}{\pi} x^{-2}. \tag{3.16}$$

This kernel appears in Figure 2 alongside thin- and a heavy- but not fat-tailed kernel. On a log-log plot fat-tailed kernels appear as straight lines, which is a result of their asymptotic convergence to power laws.

It is worth noting that when a fat-tailed kernel is rescaled, for example by setting $\widehat{k}(x) = 2k(2x)$, we obtain the same degree of tail fatness:

$$\widehat{k}(x) = \frac{2b}{\pi\left[b^2 + (2x)^2\right]} \sim \frac{2b}{\pi}(2x)^{-2} = \frac{b}{2\pi} x^{-2}. \tag{3.17}$$

Although fat-tailed kernels can be rescaled, which can affect their shape, their tails are always proportional to a standard decaying power law.

Fat-tailed distributions are always heavy-tailed, but not all heavy-tailed distributions are fat. An example of a heavy-tailed kernel that is not fat-tailed is the exponential square-root (3.12). This kernel decays slower than any exponential and so lacks a moment generating function, but faster than any power law.

In the ecological literature kernels are often distinguished as either thin-tailed or fat-tailed. In truth, the opposite of a thin-tailed kernel is a heavy-tailed kernel: thin-tailed distributions possess moment generating functions,

whereas heavy-tailed do not, and these two categories account for all (symmetric) kernels. The use of thin- and fat- to describe these complementary sets is presumably because "fat" is linguistically the opposite of "thin." Fat-tailed kernels have a much more specific form: their tails asymptotically decay like power laws.

3.3. Regularly varying densities

Fat-tailed distributions have a specific form but are still general enough to capture a wide variety of distributions. A yet more general form is that of regularly varying densities. These densities are built around the concepts of *slow* and *regular variation*.

A positive, measurable function $g(x)$ is *slowly varying* (at infinity) if for all $t > 0$,

$$\lim_{x\to\infty} \frac{g(tx)}{g(x)} = 1. \tag{3.18}$$

Slowly varying functions include positive constants and functions whose limits are positive constants, but also functions that grow sufficiently slowly, such as the logarithm (Bingham et al., 1987).

$$\lim_{x\to\infty} \frac{\log(tx)}{\log x} = \lim_{x\to\infty} \frac{\log t + \log x}{\log x} = 1, \tag{3.19}$$

$$\lim_{x\to\infty} \frac{(tx)^p}{x^p} = \lim_{x\to\infty} t^p \neq 1. \tag{3.20}$$

Power-law growth and decay form the basis for extension of slow variation to regular variation. A function $g(x)$ is *regularly varying with index* p, if for all $t > 0$,

$$\lim_{x\to\infty} \frac{g(tx)}{g(x)} = t^p. \tag{3.21}$$

Slowly varying functions are therefore technically regularly varying functions with index $p = 0$. An equivalent formulation of regular variation is that if $g(x)$ is a regularly varying function then

$$g(x) = x^p L(x) \tag{3.22}$$

for some slowly varying function $L(x)$. Regular variation can therefore be thought of as a power law multiplying a slowly varying function – a form more general than asymptotic equivalence to a power law.

Regularly varying functions permit greater variety in functional forms than asymptotic equivalence. An example of a regularly varying function that is not asymptotically equivalent to a power law is $g(x) = x^{-2}\log x$. $g(x)$ is regularly varying with index $p = -2$ since $\log x$ is slowly varying. For asymptotic equivalence to x^{-2}, the limit $g(x)/x^{-2}$ must tend to one, but

$$\lim_{x\to\infty} \frac{g(x)}{x^{-2}} = \lim_{x\to\infty} \frac{x^{-2}\log x}{x^{-2}} = \infty. \tag{3.23}$$

On the other hand, suppose that $g(x)$ is asymptotically equivalent to a power-law function, $g(x) \sim x^p$. This means that

$$\lim_{x\to\infty} \frac{g(x)}{x^p} = 1 \qquad \lim_{x\to\infty} \frac{g(tx)}{(tx)^p} = 1, \quad t > 0. \tag{3.24}$$

By applying limit laws, we have

$$\lim_{x\to\infty} \frac{g(tx)}{g(x)} = \lim_{x\to\infty} \left[\frac{g(tx)}{(tx)^p}\right]\left[\frac{x^p}{g(x)}\right] t^p = t^p, \tag{3.25}$$

from which we conclude that $g(x)$ is regularly varying with index p. We now see that the class of regularly varying functions encapsulates the class of power-law functions.

So far we have discussed regularly varying *functions*, but we now narrow our view to regularly varying *densities* – those probability distributions with pdfs that are regularly varying. We can now take advantage of results for regularly varying densities to study fat-tailed dispersal kernels – those kernels that follow power-law decay. For our purposes, the most useful results are due to Bingham et al. (2006), who studied the convolutions of regularly varying densities. If $g(x)$ and $h(x)$ are probability densities on the real line that are regularly varying at ∞, then the convolution $(g*h)(x)$ satisfies (Bingham et al., 2006),

$$(g*h)(x) \to g(x) + h(x), \qquad x \to \infty, \tag{3.26}$$

and thus is also regularly varying. This implies that the convolution of a regularly varying density $g(x)$ with itself has the simple asymptotic approximation

$$(g*g)(x) \to 2g(x), \qquad x \to \infty. \tag{3.27}$$

Furthermore, since $(g*g)(x)$ is also regularly varying, we can conclude by induction that the n-fold convolution or *convolution-power* (Feller, 1971) of $g(x)$ satisfies

$$\begin{aligned}(g^{n*})(x) &= \big(\overbrace{g*g*\cdots*g}^{n\text{-many}}\big)(x) \\ &\sim ng(x), \qquad x \to \infty.\end{aligned} \tag{3.28}$$

Further, if $g(x)$ and $h(x)$ are probability densities on the real line with $g(x)$ regularly varying and $h(x) = o(g(x))$ as $x \to \infty$, then their convolution has the property (Bingham et al., 2006)

$$(g*h)(x) \to g(x), \qquad x \to \infty. \tag{3.29}$$

The notation $h(x) = o(g(x))$ means that $g(x)$ *dominates* $h(x)$ such that

$$\lim_{x\to\infty} \frac{h(x)}{g(x)} = 0. \tag{3.30}$$

The density function $g(x)$ has, in effect, a heavier tail than $h(x)$ if it dominates $h(x)$. The property (3.29) is useful because $h(x)$ need not be regularly varying, and can for example be thin-tailed.

Although we have stressed that regularly varying densities are a broader set of kernels than fat-tailed ones, throughout the remainder of this paper we will focus exclusively on fat-tailed ones. From a modeling perspective, fat-tailed kernels are common and come in sufficient variety that this is not unduly restrictive. Our purpose for introducing regularly varying densities is to take advantage of their useful tail additivity properties when dealing with the more restrictive fat-tailed case. Nevertheless, extension of our work to regularly varying densities would be a useful endeavor and potential area of future work.

3.4. Example fat-tailed kernels

To perform numerical experiments we must select particular or example fat-tailed kernels. We chose kernels based on two well-known thin-tailed kernels: the Gaussian and Laplace distributions. These kernels have qualitatively different shapes at the origin: the Gaussian has a smooth, round shape and the Laplace kernel is peaked. The fat-tailed Gaussian has round profile similar to the Gaussian, and the fat-tailed Laplace kernel has a peak like the Laplace kernel. These kernels are shown in Figure 3 alongside their thin-tailed counterparts.

The fat-tailed Gaussian is Student's t-distribution. The t-distribution is a well-known fat-tailed density that is commonly used in statistical tests. A two-dimensional variant, the 2Dt distribution, has been developed and used in ecological modeling (Clark et al., 1999; Bullock et al., 2017). We retain the standard parameterization with $\nu \geq 1$ measuring the "degrees of freedom"; the order of tail fatness is $\alpha = \nu + 1$.

$$k(x) = \frac{\Gamma\left(\frac{\nu+1}{2}\right)}{\Gamma\left(\frac{\nu}{2}\right)\sqrt{\nu\pi}}\left(1+\frac{x^2}{\nu}\right)^{-\left(\frac{\nu+1}{2}\right)}. \tag{3.31}$$

As $\nu \to \infty$, the t-distribution converges to the standard normal distribution, but it retains its fat tails for all finite ν. For $\nu = 1$, the t-distribution becomes the Cauchy distribution (3.10).

The fat-tailed Laplace kernel,

$$k(x) = \frac{\alpha - 1}{2\alpha\left(1 + |x|/\alpha\right)^{\alpha}}. \tag{3.32}$$

is based on the two-dimensional "geometric" or "power-law" kernel (Nathan et al., 2012). The kernel (3.32) is a well-defined probability density for $\alpha > 1$, but it may have infinite variance. For $\alpha > 3$, the geometric kernel has finite variance. As $\alpha \to \infty$, the fat-tailed Laplace kernel converges to the Laplace kernel, but for all finite values of α, the kernel has fat tails whereas the Laplace kernel is thin-tailed.

We remark that these kernels are members of larger classes of kernels. The Gaussian and Laplace kernels are both special cases of the *exponential power* (Kotz et al., 2001) or *generalized normal* distribution,

$$k(x) = \frac{\beta}{2\alpha\Gamma(1/\beta)}e^{-(|x|/\alpha)^{\beta}}. \tag{3.33}$$

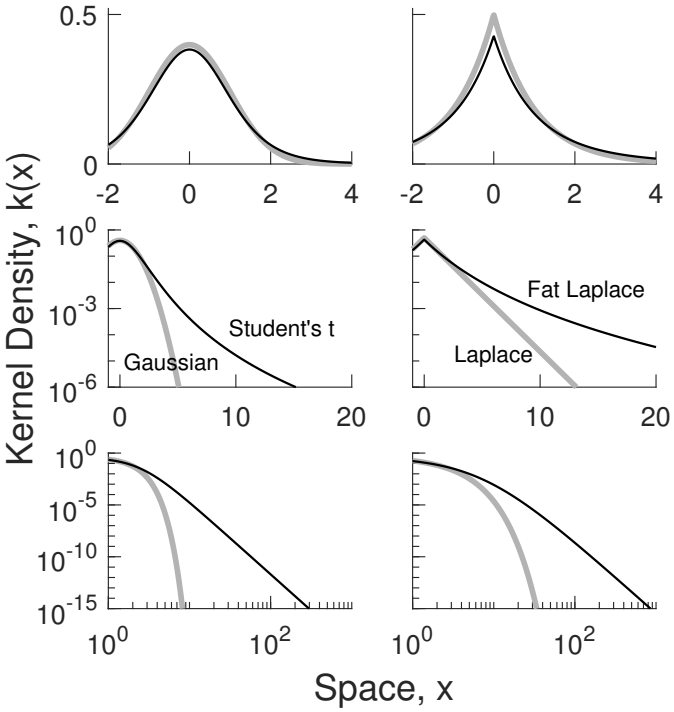

Figure 3: Fat-tailed kernels used in numerical simulations. **(Left)** The fat-tailed Gaussian kernel (Student's t-distribution) alongside its thin-tailed counterpart, the Gaussian distribution. The kernels appear quite similar in linear scales, with similar rounded shapes. In linear-log scale, the difference in the tails is more evident, as the Gaussian decays rapidly while the t-distribution decays at a slowing rate. In log-log scale, the tails of the t-distribution tend to straight lines because they converge to power laws. **(Right)** The fat-tailed Laplace kernel and the (thin-tailed) Laplace kernel. Both have a peaked shape at the origin, but differ in the tails similarly to the Gaussian and t-distribution.

The exponential power distribution has been used in ecological modeling of pollen dispersal (Nathan et al., 2012). The fat-tailed Laplace kernel and t-distribution are themselves special cases of the *generalized Cauchy distribution* (Miller and Thomas, 1972), which is a fat-tailed analogue of the exponential power family in the same manner in which the t-distribution is the fat-tailed analogue of the Gaussian. The generalized Cauchy distribution has a parameter ν for controlling tail fatness, as well as a parameter c analogous to β in equation (3.33) that controls the tail heaviness of the limiting distribution.

Using these as our example kernels has several benefits. Primarily, we can compare against the known behavior of the Gaussian and Laplace kernels. The Gaussian and Laplace kernels are both thin-tailed kernels whose invasion speeds have been well-characterized. They are known to have different invasion speeds, with the Laplace kernel outstripping a Gaussian kernel of equal variance for the same net reproductive rate R_0. As we will see, the invasion speeds of the thin-tailed kernels do affect their fat-tailed counterparts.

4. Point-release initial conditions

A point-release invasion begins with a small population initially confined to a small area, approximated by a point. A point-release invasion describes a newly emerging population, sometimes starting from transplanted individuals or from a long-distance dispersal event that has carried a propagule a far distance from its source.

In this section we derive a formal solution to the linear integrodifference equation (2.3) in terms of convolutions of the kernel and use tail additivity to obtain a tail approximation. We assume general power-law decay of the kernel (fat tails) to find the rate of invasion. We then develop a more sophisticated analysis based on scaling arguments and analogies to probability densities that allows us to draw the same conclusions for the nonlinear model, including when the growth function has a weak Allee effect.

4.1. Linear model

When the initial condition is a point release, we can approximate it as a *delta function*, $\delta(x)$. The delta function is defined as a *generalized function* that integrates to one,

$$\int_{-\infty}^{\infty} \delta(x)\mathrm{d}x = 1, \tag{4.1}$$

and which is zero everywhere except at the origin,

$$\delta(x) = 0 \quad \text{for all } x \neq 0. \tag{4.2}$$

The delta function is not a true function, since it has no well-defined value at the origin. It can be thought of as the limit of increasingly narrow Gaussian distributions, concentrating total probability on the origin.

A key property of the delta function is the *sifting property* (Bracewell, 1986),

$$\int_{-\infty}^{\infty} f(x-y)\delta(y)\mathrm{d}y = f(x). \tag{4.3}$$

This property essentially states that the delta function is the function that preserves any other function under convolution. This is immediately useful to us: if the initial population density is localized to a point and N_0 is the number of individuals or *source strength*, then the initial condition can be modeled with a delta function, $n_0(x) = N_0\delta(x)$, and we can easily find the first generation $n_1(x)$ under the linear model (2.3),

$$\begin{aligned} n_1(x) &= N_0 R_0 \int_{-\infty}^{\infty} k(x-y)\delta(y)\mathrm{d}y \\ &= N_0 R_0 k(x). \end{aligned} \tag{4.4}$$

We remark that the use of the delta function as an initial condition is not always valid. In the nonlinear model, where we must compute $f(n_0(x))$, a delta function initial condition poses a problem because $\delta(0)$ has no defined value, and so $f(\delta(0))$ likewise has no defined value (**?**). In the present case, using a delta function is permissible because of the simplified form of the linear model that reduces to a convolution. Indeed, the action of the delta function is defined in terms of a convolution-type integral (**?**).

The simple form of $n_1(x)$ in terms of the kernel allows us to find an exact formal solution of the linear model in terms of self-convolutions of the kernel,

$$\begin{aligned} n_t(x) &= N_0 R_0^t \big(\overbrace{k * k * \cdots * k}^{t\text{-many}}\big)(x) \\ &= N_0 R_0^t k^{t*}(x). \end{aligned} \tag{4.5}$$

Even given the form of $k(x)$, the convolution $(k * k)(x)$ may be difficult or impossible to find in closed form, and further convolutions are yet more difficult to obtain.

Assuming that $k(x)$ is regularly varying, we can make much progress. By the tail additivity property (3.28), we have $k^{t*}(x) \sim tk(x)$, and so we obtain the asymptotic equivalence

$$n_t(x) \sim N_0 R_0^t t k(x), \qquad x \to \infty. \tag{4.6}$$

This tells us that the tail of $n_t(x)$ is the same as that of the dispersal kernel $k(x)$, but scaled by a factor of $N_0 R_0^t t$. Given the form of the kernel $k(x)$ we can in principle invert the kernel to recover the position of the invasion front.

Figure 4 shows the true and approximate solutions, equations (4.5) and (4.6), for a point-release invasion under the linear model. We see that at standard linear scales, the approximation is not particularly convincing. Shifting to log scale, the approximation clearly coincides with the true solution for large x in the tails. We also see that successive generations have tails of increasing magnitudes: this is the factor $R_0^t t$ in equation (4.6).

4.2. Rate of invasion for fat-tailed kernels

Without knowing the specific kernel form, we can make much headway by assuming general power-law decay. Let $\overline{N}$ denote a threshold value, and let x_t be the position of the invasion front at time t, so that the invasion front and threshold value are related by

$$n_t(x_t) = \overline{N}. \tag{4.7}$$

That is, the population density at the invasion front is the threshold value. Then at successive front positions, we have

$$n_{t+1}(x_{t+1}) = n_t(x_t) = \overline{N}. \tag{4.8}$$

Applying approximation (4.6), we have

$$N_0 R_0^{t+1}(t+1)k(x_{t+1}) \approx N_0 R_0^t t\, k(x_t) \tag{4.9}$$

so

$$R_0\left(\frac{t+1}{t}\right) k(x_{t+1}) \approx k(x_t). \tag{4.10}$$

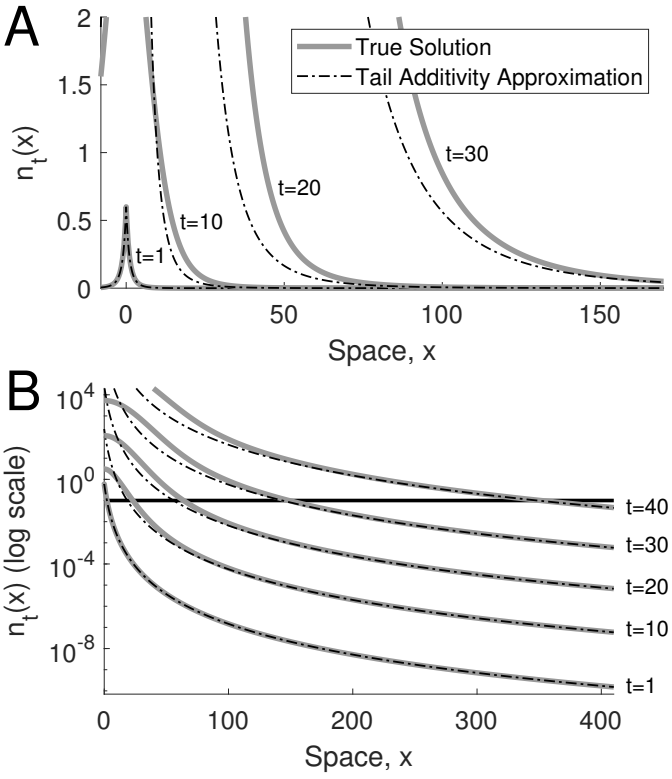

Figure 4: True solution and tail additivity approximation for the linear model. **(A)** The true solution (gray lines) and approximation (4.6) due to tail additivity (black dashed-dotted lines) at times $t = 1, 10, 20, 30$. Dispersal is according to the fat-tailed Laplace kernel (3.32) with tail fatness $\alpha = 5$ and $R_0 = 1.5$. **(B)** In log-space the tail addivitity approximation is seen to be accurate in the tails. The solid black line corresponds to the fixed detection threshold $\overline{N} = 0.1$, a typical value used to measure the extent of the invasion.

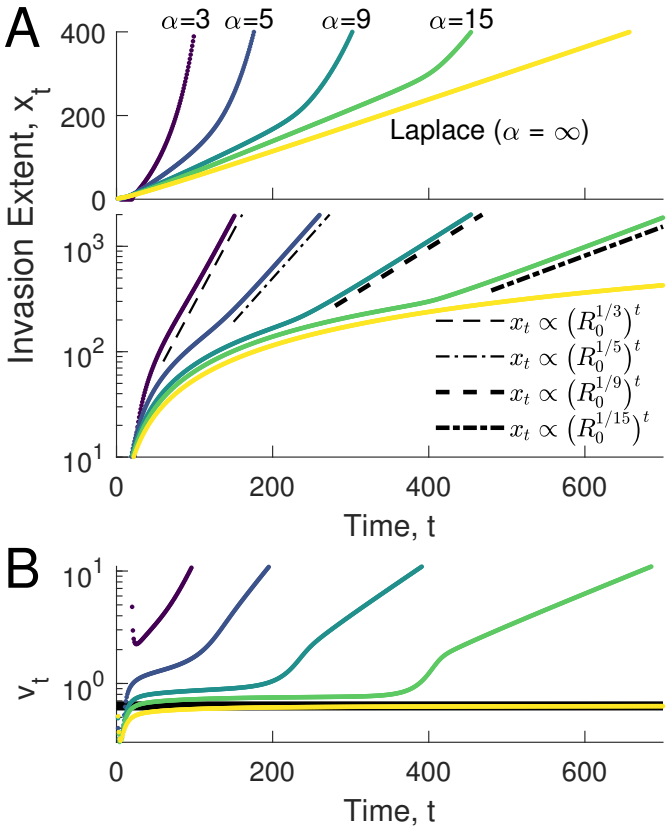

Figure 5: Rates of spread for fat-tailed invasions. Plots show the invasion extent x_t in both linear and logarithmic scales, as well as the invasion speed v_t for invasions with fat-tailed Laplace-kernel dispersal with $\alpha = 3, 5, 9, 15$. Also shown is invasion according to Laplace-kernel dispersal. **(A)** Fat-tailed invasions exhibit a transient phase of constant invasion speed during which the invasion progresses at a linear rate of spread. Plotting the invasion extent in log space reveals straight line trends, indicating geometric growth. The long-term or asymptotic rate of spread for fat-tailed point-release invasions is geometric with base $R_0^{1/\alpha}$. **(B)** Plotting the per-step invasion speed $v_t = x_t - x_{t-1}$ shows that the invasion speed during the constant speed transient is closely related to the spreading speed of the Laplace kernel (black line).

Now assume that $k(x) \sim cx^{-\alpha}$ is a fat-tailed probability density function. We then obtain

$$x_{t+1}^{\alpha} \approx R_0 \left(\frac{t+1}{t}\right) x_t^{\alpha}. \tag{4.11}$$

For large t the factor $(t+1)/t$ becomes negligible and we observe geometric growth of the invasion front:

$$x_{t+1} \approx R_0^{1/\alpha}\, x_t, \qquad t \to \infty. \tag{4.12}$$

We say that such an invasion has a *geometric rate of spread*, with *base* $R_0^{1/\alpha}$. For an in-depth discussion of this approach for finding the invasion rate, please see the discussion in *Accelerating waves*.

It is important to note that the tail additivity property that we rely on in these arguments is an asymptotic relation, meaning that it holds as x becomes large. What this precisely means in terms of rates of convergence or when the relation can be said to hold 'well' depends on the distribution and parameters. A general rule is that as R_0 is made larger, the spatial extent grows more rapidly, moving the front position further into the tail of the distribution faster, where the asymptotics hold best.

4.3. Numerical examples

Numerical simulations are a natural complement to traditional analysis, especially in our case where our main results are asymptotic and deal with large time. Numerical examples enlighten us as to the early-time or transient dynamics that dominate spread rates in the early stages of invasion before the asymptotic dynamics take effect.

In our simulations, the domain is a large interval, with half-width H, centered about the origin, represented by a grid of points with uniform spacing Δx. The population densities $n_t(x)$ and the dispersal kernel $k(x)$ are represented on this domain, effectively truncating any infinite tails. Edge effects from the boundaries of the domain can affect the progress of an invasion front, so a buffer is afforded when selecting the width of the domain and simulations are re-run if the invasion front tends too close to either boundary. For the nonlinear model we use the Beverton–Holt growth function (Beverton and Holt, 1957), except

in the section *Weak Allee effects* where we use specialized growth functions with weak Allee effects. Point-release initial conditions for the nonlinear model were specified by setting $n_t(x) = N_0$, the source strength, for all gridpoints x_j satisfying $-1/2 < x_j < 1/2$ and $N_0/2$ for $|x_j| = 1/2$.

Our simulations are implemented in MATLAB. We use a midpoint rule integration scheme for computing convolutions. This rule is implemented by the numerical convolution command `conv` with the `'same'` option, which computes a numerical convolution of two vectors truncated to the same length as the starting vector. To measure population extent by a threshold value $\overline{N}$ we used the `find` command to select the last grid point x_j satisfying $n_t(x_j) > \overline{N}$. We then used interpolation with the `interp1` command with the `'spline'` method (cubic spline interpolation) on the surrounding points $x_{j-1}, \ldots, x_{j+2}$ to compute an accurate estimate of the invasion extent x_t such that $n_t(x_t) = \overline{N}$.

Figure 5 shows invasion extent x_t over time for five point-release invasions. In each invasion, the net reproductive rate is $R_0 = 1.1$, and the dispersal kernel is the fat-tailed Laplace kernel (3.31) with $\alpha = 3, 5, 9, 15$. Also plotted is the invasion with Laplace-kernel (thin-tailed) dispersal for comparison. The plots reveal several key facts. First, the invasions have initial or transient periods where they progress at near linear rates of spread or constant speeds. Second, as α increased, the invasions coincide more closely with the invasion with Laplace-kernel dispersal, at least in the short term. Third, asymptotically or in the long term, the invasions spread at geometric rates. We now address each of these points.

The *constant speed transient* period is perhaps the most noticeable feature of fat-tailed invasions. When x_t is plotted versus time in linear scale the trend is initially linear, similar to thin-tailed or constant speed invasions. We see that as α is increased, the duration of the constant speed transient is increased. This is related to the second observation: that the invasions begin to coincide with the thin-tailed invasion. We have already remarked that as $\alpha \to \infty$, the fat-tailed Laplace kernel converges to the Laplace kernel; this means that in a way, their invasions also converge. The invasion speed during the constant speed transient is finite and for our families of fat-tailed kernels can be related to their thin-tailed limiting distributions: the Gaussian for the t-distribution and the Laplace kernel for the fat-tailed Laplace kernel.

4.4. Nonlinear model

The previous point-release analysis is limited in that it is based on the linear model, and so by conventional reasoning does not apply to invasions with weak Allee effects where the linear conjecture does not hold. In this section we carry out an alternative analysis, now with the nonlinear model. The general approach is to make mild assumptions on the initial condition and growth function such that each generation of the nonlinear model resembles a probability density function (pdf). By scaling each

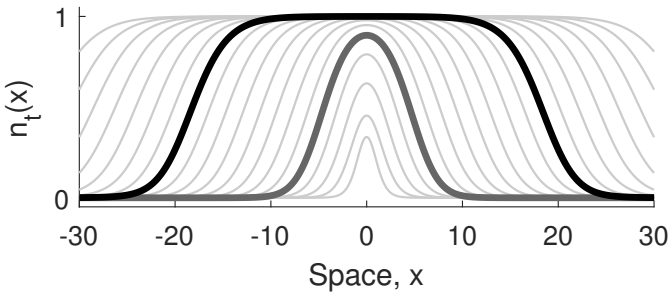

Figure 6: Population densities viewed as probability densities. Point-release invasions have population density profiles $n_t(x)$ that are scaled probability density functions (pdfs). By rescaling the generations $n_t(x)$ we obtain pdfs, to which we can apply asymptotic tail additivity laws.

generation $n_t(x)$ by its total area we obtain probability densities (Figure 6) and can use the tail additivity properties of regularly varying densities. We find that the tails of $n_t(x)$ again mirror those of the dispersal kernel, and obtain the same asymptotic invasion rate of geometric growth as in the linear model.

We consider the nonlinear model (2.2) with point-release initial condition. We assume that $R_0 = f'(0) > 1$ so that there is at most a weak Allee effect and that $f(n)$ has fixed points $n^* = 0$, unstable, and $n^* = 1$, a stable equilibrium. Assuming that the initial condition has compact support, so that $n_0(x) = 0$ outside of a bounded interval, each generation $n_t(x)$ will tend to zero for $|x|$ large, be bounded above by the carrying capacity, and integrate to a finite number. Thus, each generation will resemble a scaled probability density.

Since a delta-function initial condition is not compatible with the nonlinear model, we must make alternative assumptions about the initial condition. Define the total number of offspring at each generation, A_t as

$$A_t = \int_{-\infty}^{\infty} f\left(n_t(x)\right) \mathrm{d}x. \tag{4.13}$$

We will assume that the initial condition $n_0(x)$ is such that $A_0 > 0$ is a well-defined real number and that the sequence $A_0, A_1, A_2, \ldots$ does not decrease. From the assumption that $n_0(x)$ has compact support we also have that $f(n_0(x))/A_0$ is technically a thin-tailed probability density function. With tail additivity theorem (3.29), we then have that

$$\begin{aligned} n_1(x) &= \left[k * f(n_0)\right](x) \\ &= A_0 \left[k * \frac{f(n_0)}{A_0}\right](x) \\ &\sim A_0 k(x). \end{aligned} \tag{4.14}$$

Here the first equality comes from the linearity of the convolution operator, and the asymptotic equivalence from theorem (3.29).

Note that $f(n_t(x))/A_t$ is a probability density since it is a positive function that integrates to one, and so can

be used in conjunction with tail additivity theorem (3.26). Also note that since $f(n) \to R_0 n$ as $n \to 0$ and $n_t(x) \to 0$ as $x \to \infty$, that $f(n_t(x)) \to R_0 n_t(x)$ as $x \to \infty$. With these facts we can find asymptotic tail approximations for the first few iterates. We first obtain $n_2(x)$,

$$\begin{aligned} n_2(x) &= [k * f(n_1)](x) \\ &= A_1 \left[k * \frac{f(n_1)}{A_1} \right](x) \\ &\sim A_1 \left[k(x) + \frac{f(n_1(x))}{A_1} \right] \end{aligned} \tag{4.15}$$

where the second equality comes from the linearity of the convolution operator, and the asymptotic equivalence from theorem (3.26). Next,

$$\begin{aligned} n_2(x) &\sim A_1 k(x) + R_0 n_1(x) \\ &\sim A_1 k(x) + R_0 A_0 k(x) \end{aligned} \tag{4.16}$$

Similarly,

$$\begin{aligned} n_3(x) &= [k * f(n_2)](x) \\ &\sim A_2 \left[k(x) + \frac{f(n_2(x))}{A_2} \right] \\ &\sim A_2 k(x) + R_0 n_2(x) \\ &\sim A_2 k(x) + R_0 A_1 k(x) + R_0^2 A_0 k(x). \end{aligned} \tag{4.17}$$

We see that the t-th generation has the asymptotic form

$$n_t(x) \sim s_t k(x) \tag{4.18}$$

with

$$\begin{aligned} s_t &= A_{t-1} + R_0 A_{t-2} + \cdots + R_0^{t-1} A_0 \\ &= \sum_{k=0}^{t-1} R_0^t A_{t-1-k}. \end{aligned} \tag{4.19}$$

If we knew A_t we could exactly predict the tail scale s_t of each generation of the population $n_t(x)$. Unfortunately it is not easy to compute the total number of offspring at each generation. By relating the total population size N_t to the number of offspring, and by bounding the total population size by the rate of spread of the invasion, we can bound the rate of invasion from below and above, ultimately finding that the nonlinear model has the same geometric rate of spread as the linear model. Details of this argument are in Appendix A.

5. Weak Allee effects

A weak Allee effect is intermediate between compensation (no Allee effect) and critical depensation (a strong Allee effect). Although a growth function either does or does not have a weak Allee effect, the invasion rate often transitions smoothly rather than sharply as an Allee effect is introduced. As an example, consider the Nagumo equation (Britton, 1986),

$$\frac{\partial u}{\partial t} = u(u-\beta)(1-u) + D\frac{\partial^2 u}{\partial x^2}. \tag{5.1}$$

The growth in (5.1) has three parameter regimes: no Allee effect for $\beta < -1$, a weak Allee effect for $-1 < \beta < 0$, and a strong Allee effect for $0 < \beta < 1$. Separate analyses find the speed of invasion for the cases of no Allee effect and strong Allee effect, and it is observed that these analyses each correctly predict the invasion speed within part of the weak-Allee regime (Lewis et al., 2016).

In this section we use simulations to analyze the rates of invasion for two families of growth functions that sit at the extremes of the weak Allee effect. The first extreme lies at the transition between the weak Allee effect and no Allee effect, and the second between weak and strong Allee effect. We find that the asymptotic results derived in the previous section do hold, but the degree of Allee effect can greatly affect the initial invasion rate and the duration of initial transient invasion speeds that precede the ultimate rate of invasion.

5.1. Transition to depensation

We first examine the transition to depensation; that is, how the rate of spread changes as a weak Allee effect is introduced. We construct a family of growth functions with a parameter γ that controls how prominent the weak Allee effect is,

$$f(n) = \begin{cases} n\left[R_0 + (R_m - R_0)(R_m n)^\gamma\right] & n < 1/R_m \\ 1 & n \geq 1/R_m. \end{cases} \tag{5.2}$$

Examples of this growth function can be seen in Figure 7 with $R_0 = 1.1$, $R_m = 4$, and values of $\gamma = 0, 2^{-4}, 2^{-3}, \ldots, 2^4$.

There are two extreme cases: when $\gamma = 0$, the growth function reduces to a piecewise linear function,

$$f(n) = \begin{cases} R_m n & n < 1/R_m \\ 1 & n \geq 1/R_m. \end{cases} \tag{5.3}$$

This growth function has net reproductive rate R_m and no Allee effect. On the other hand, as $\gamma \to \infty$, the function converges to a different piecewise linear function,

$$f(n) = \begin{cases} R_0 n & n < 1/R_m \\ 1 & n \geq 1/R_m. \end{cases} \tag{5.4}$$

This growth function has net reproductive rate R_0, but has maximum per capita recruitment R_m, attained at $n = 1/R_m$.

For values of $0 < \gamma < \infty$, growth function (5.2) has behavior between these cases. The function has the value $f(1/R_m) = 1$ and therefore has maximum per capita recruitment R_m attained at the point $n = 1/R_m$; however, $f'(0) = R_0$, and so an Allee effect is always present.

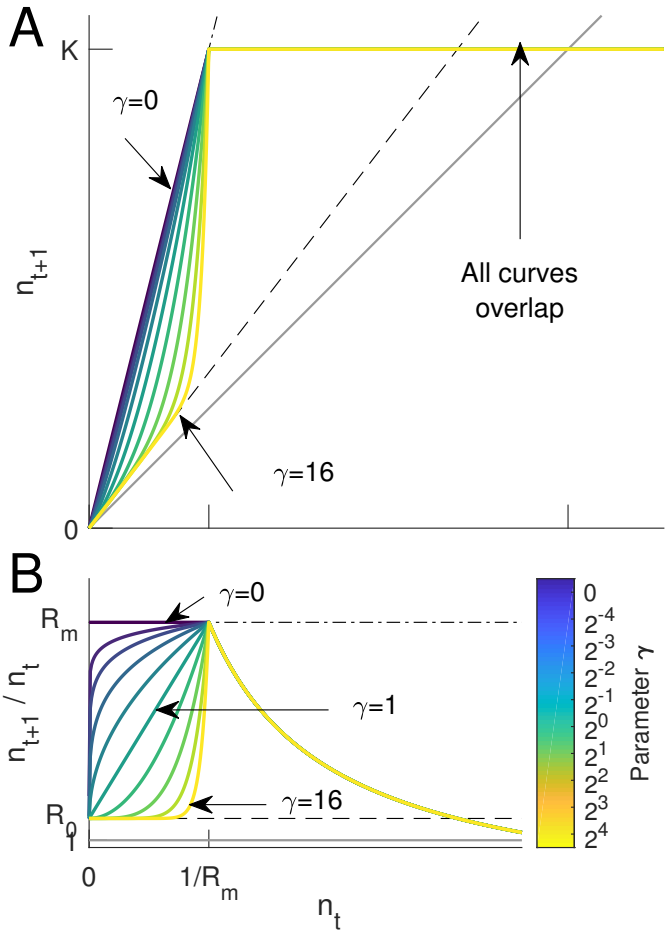

Figure 7: Weakening a weak Allee effect. **(A)** The family of growth functions (5.2) smoothly encompasses the cases of no Allee and weak Allee effect. Curves shown are the function with parameter values $\gamma = 0, 2^{-4}, 2^{-3}, \ldots, 2^4$. For $\gamma = 0$, the growth function has no Allee effect and the net reproductive rate is R_m. For $\gamma > 0$, the net reproductive rate is R_0. **(B)** The per-capita recruitment n_{t+1}/n_t.

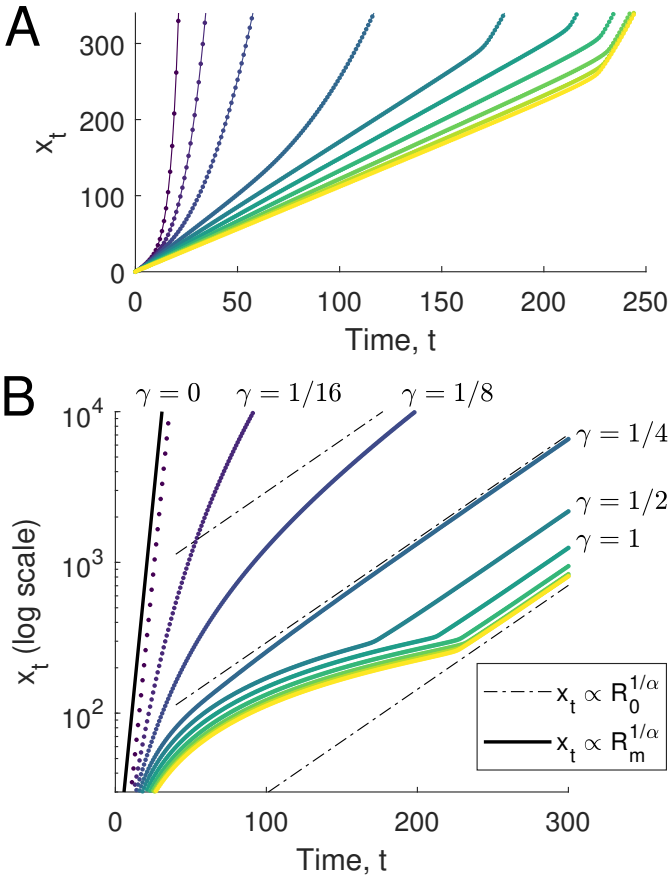

Figure 8: Rates of invasion as a weak Allee effect is introduced. **(A)** The invasion extent over time of ten simulations with the growth functions shown in Figure 7 with $R_0 = 1.1$ and $R_m = 4$. In all simulations the dispersal kernel is the t-distribution with $\nu = 5$. As γ is increased, the strength of the Allee effect is increased and the constant speed transient becomes pronounced. As γ is reduced, the Allee effect is weakened and the invasion has a faster initial rate of spread. **(B)** Viewed in a logarithmic scale, the asymptotic rate of spread of spread can be more clearly seen. For larger values of γ we see geometric growth with base $R_0^{1/\alpha}$.

Populations that grow under these growth functions invade very differently depending on the degree of the weak Allee effect, as can be seen in Figure 8. For $\gamma = 0$, the population invades rapidly at a geometric rate with base $R_m^{1/\alpha}$, which is expected, since in this case the growth function has no Allee effect and has net reproductive rate R_m. On the other hand, for $\gamma = 1/2, 1, 2, 4, 8, 16$, the populations exhibit constant speed transients for over one hundred iterations before transitioning to invasion at a geometric rate with base $R_0^{1/\alpha}$. For $0 < \gamma < 1/2$ the invasions initially invade rapidly and faster than geometrically with base $R_0^{1/\alpha}$, but the trends indicate a slowing rate of invasion that converges to geometric with base $R_0^{1/\alpha}$. Thus our asymptotic result — that the invasions will converge to a geometric rate of spread with base $R_0^{1/\alpha}$ — holds, but the rate of convergence can be made very slow by careful choice of growth function.

5.2. *Transition to critical depensation*

We now address the case of weak Allee effects that border on the strong Allee case. In a strong Allee effect $R_0 < 1$, so this case can be thought of as strengthening a weak Allee effect such that $R_0 > 1$ approaches one. We construct a family of growth functions with an Allee effect where R_0 can be made close to one,

$$f(n) = \frac{R_0 n}{1 + (2 - R_0 - bR_0)n + (1 - bR_0)n^2}. \qquad (5.5)$$

This growth function satisfies $f'(0) = R_0$ and $f'(1) = b$. For our simulations we set $b = .5$ and $R_0 = 1.1, 1.01, 1.001$. As we will soon see, the invasions that result from near-strong weak Allee effects have extremely long transient dynamics, so this growth function was selected to ensure that each generation $n_t(x)$ was smooth to allow for simulations and numerical integration on a coarse numerical grid.

Figure 9 shows plots of the invasion extent for the three invasions with $R_0 = 1.1, 1.01, 1.001$. For all three simulations we observe an initial constant speed transient that gives way to geometric growth. As R_0 is decreased to one the duration of the constant speed transient lengthens, delaying the geometric phase; for $R_0 = 1.001$ the transient phase lasts for nearly 15 000 generations. In all cases the asymptotic rate of spread is geometric with base $R_0^{1/\alpha}$.

We remark that in the limit as $R_0 \to 1$, then $R_0^{1/\alpha} \to 1$ as well, which marks a breakdown in both our analysis as well as the analytic result: when the base of the exponent becomes one, there is no longer geometric growth. Thus the case where $R_0 = 1$ can be seen as a limiting case in two ways: first, the duration of the constant speed transient becomes infinite, and second, the geometric growth phase becomes degenerate.

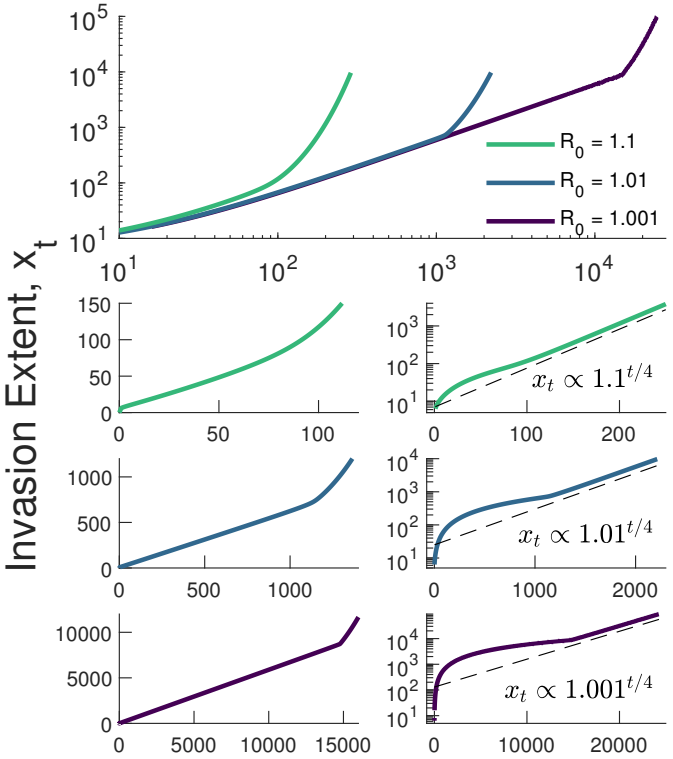

Figure 9: Acceleration of invasions is delayed as a weak Allee effect is strengthened. Invasions with near-strong weak Allee effects have extremely long periods of nearly-constant invasion speeds. Plots show invasion extent over time for point-release invasions with the weak Allee growth function (5.5) with $R_0 = 1.1, 1.01, 1.001$. Dispersal is according to the t-distribution with $\nu = 5$. The constant speed transient period lengthens as R_0 is reduced but the (eventual) asymptotic rate of spread is always geometric with base $R_0^{1/\alpha}$. For the case where $R_0 = 1.001$ the invasion progresses at a near-constant invasion speed for over 14 000 generations before transitioning to geometric growth. In all simulations the grid spacing is $\Delta x = 0.5$; the domain half-width is $H = 10\,000$ for $R_0 = 1.1, 1.01$ and $H = 100\,000$ for $R_0 = 1.001$.

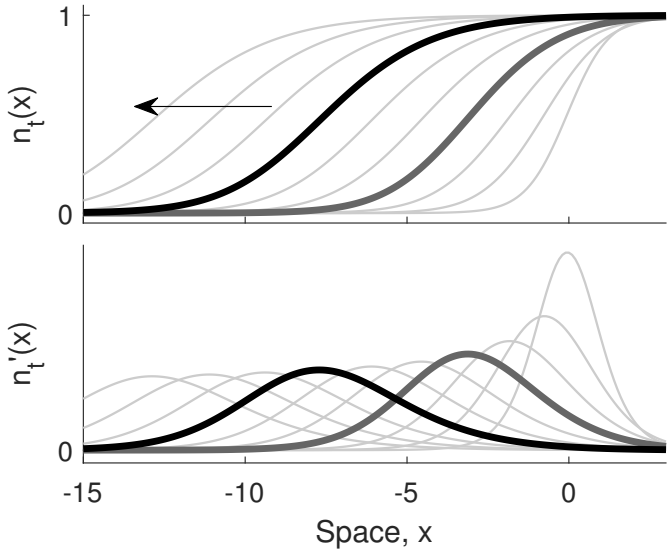

Figure 10: Population densities viewed as distribution functions. The generations $n_t(x)$ of a front-release invasion can be viewed as cumulative distribution functions (cdf). Their derivatives $n_t'(x)$ can then be viewed as probability density functions (pdf).

6. Front-release initial conditions

We now turn to invasion following front-release initial conditions, where well-established populations invade new territory. To simplify our arguments and analysis we assume that the population carrying capacity has been re-scaled to one and restrict our attention to leftward-moving invasions. We derive a tail approximation for a front-release invasion under the nonlinear model, and then use it to find the rate of invasion.

The general approach is to make mild assumptions on the initial condition and growth function such that each generation of the nonlinear model resembles a cumulative distribution function. Figure 10 shows example front-release generations: $n_t(x)$ goes from zero at $-\infty$ to one (the rescaled carrying capacity) at $+\infty$, satisfying the conditions of a cumulative distribution function. This also means that the derivative, $n_t'(x)$, is a probability density function. Through transformations we recast the nonlinear model as an iteration that moves between cumulative distributions and probability densities, and we track the shape and scale of the tails of these distributions.

To proceed we must also make some assumptions about the growth function $f(n)$. In addition to $f(n)$ being monostable with $n = 0$ unstable and $n = 1$ stable, we assume that $f(n)$ has at most a weak Allee effect and is also *order-preserving*; this means that if $n \le m$, then $f(n) \le f(m)$. From these assumptions, we can conclude that if $n_t(x)$ is a cdf, then $f(n_t(x))$ is also a cdf.

6.1. Tail approximation

Consider again the nonlinear model,

$$n_{t+1}(x) = [k * f(n_t)](x). \tag{6.1}$$

The process to obtain $n_{t+1}(x)$ from $n_t(x)$ can be succinctly expressed in terms of *operators*. Let $\mathbf{f}$ represent application of the growth function $f(n)$ to every point in the domain,

$$(\mathbf{f}n_t)(x) = f\left(n_t(x)\right) \tag{6.2}$$

and $\mathbf{k}$ represent convolution with the dispersal kernel $k(x)$,

$$(\mathbf{k}\mathbf{f}n_t)(x) = (k * \mathbf{f}n_t)(x) = \left[k * f(n_t)\right](x). \tag{6.3}$$

The *operators* $\mathbf{f}$ and $\mathbf{k}$ act on functions of x to produce new functions of x. The function $n_{t+1}(x)$ can be expressed by applying $\mathbf{f}$ to $n_t(x)$ and by then applying $\mathbf{k}$ to get

$$n_{t+1}(x) = \mathbf{k}\mathbf{f}n_t(x). \tag{6.4}$$

Operator notation is convenient for expressing more complicated operations. Consider differentiation and integration: both act on functions of x and return functions of x, and so are operators. Let $\mathbf{D}_x$ denote differentiation with respect to space,

$$(\mathbf{D}_x n_t)(x) = \frac{\mathrm{d}}{\mathrm{d}x} n_t(x) \tag{6.5}$$

and $\mathbf{D}_x^{-1}$ definite integration from $-\infty$ to x,

$$(\mathbf{D}_x^{-1} n_t)(x) = \int_{-\infty}^{x} n_t(y)\mathrm{d}y. \tag{6.6}$$

Assuming that the original function $n_t(x)$ has the limit $n_t(x) \to 0$ as $x \to -\infty$, then these two operators act as inverses of one another,

$$\mathbf{D}_x^{-1}\mathbf{D}_x n_t = n_t. \tag{6.7}$$

That is, if we differentiate $n_t(x)$ and then integrate the result, we re-obtain $n_t(x)$. These operators can also be related to the kernel pdf and cdf: $k = \mathbf{D}_x K$ and $K = \mathbf{D}_x^{-1} k$.

With these operators in place, we can rewrite the nonlinear model as

$$\begin{aligned} n_{t+1} &= \mathbf{k}\mathbf{D}_x^{-1}\mathbf{D}_x\mathbf{f}n_t \\ &= \mathbf{D}_x^{-1}\mathbf{k}\mathbf{D}_x\mathbf{f}n_t. \end{aligned} \tag{6.8}$$

where the rearrangement of the integration $\mathbf{D}_x^{-1}$ and the convolution $\mathbf{k}$ in the second line is allowed by the fact that both are linear operators that commute with one another. The added steps of differentiation and integration can be viewed as transformations that move between a space of cumulative distribution functions (that correspond to population density profiles) and probability density functions. The advantage of breaking up the iteration in this way is that each of the operations, $\mathbf{f}, \mathbf{D}_x, \mathbf{k}, \mathbf{D}_x^{-1}$ can be understood separately in terms of their affect on the tail of the population density.

This decomposition will allow us to track how the tail of the population evolves, but first we must specify an initial condition. The simplest front-like initial condition is the *Heaviside function*,

$$n_0(x) = H(x) = \begin{cases} 0 & x < 0 \\ 1 & x \geq 0. \end{cases} \tag{6.9}$$

When the initial population density is given by the Heaviside function the population density of the first generation will be given by the cdf $K(x)$ of the dispersal kernel. This is because

$$\begin{aligned} n_1(x) &= \int_{-\infty}^{\infty} k(y)H(x-y)\mathrm{d}y \\ &= \int_{-\infty}^{x} k(y)\mathrm{d}y \\ &= K(x). \end{aligned} \tag{6.10}$$

Using the iteration (6.8) and tracking the intermediate results, we first apply the growth function,

$$\begin{aligned} \left(\mathbf{f}n_1\right)(x) &= f\left(n_1(x)\right) \\ &\sim R_0 K(x), \qquad x \to -\infty, \end{aligned} \tag{6.11}$$

then differentiate with respect to x,

$$\begin{aligned} \left(\mathbf{D}_x\mathbf{f}n_1\right)(x) &\sim R_0\mathbf{D}_x n_1(x) \\ &\sim R_0 k(x), \end{aligned} \tag{6.12}$$

convolve by the dispersal kernel,

$$\begin{aligned} \left(\mathbf{k}\mathbf{D}_x\mathbf{f}n_1\right)(x) &= \mathbf{k}\left[R_0 k(x)\right] \\ &\sim R_0 k(x) + k(x) \\ &= (R_0+1)k(x), \end{aligned} \tag{6.13}$$

and finally integrate from $-\infty$,

$$\begin{aligned} \left(\mathbf{D}_x^{-1}\mathbf{k}\mathbf{D}_x\mathbf{f}n_1\right)(x) &= \mathbf{D}_x^{-1}(R_0+1)k(x) \\ n_2(x) &\sim (R_0+1)K(x). \end{aligned} \tag{6.14}$$

In the above all asymptotic relations hold as $x \to -\infty$ because we are examining a leftward-moving wave. We see that the first iterate has tail decay matching the cdf $K(x)$, and the second has the same degree of tail decay but multiplied by a factor of (R_0+1).

Repeating this for the third,

$$\begin{aligned} n_3(x) &\sim \left[R_0(R_0+1)+1\right]K(x) \\ &= \left(R_0^2 + R_0 + 1\right)K(x), \end{aligned} \tag{6.15}$$

and fourth iterate,

$$\begin{aligned} n_4(x) &\sim \left[R_0(R_0^2+R_0+1)+1\right]K(x) \\ &= \left(R_0^3 + R_0^2 + R_0 + 1\right)K(x). \end{aligned} \tag{6.16}$$

we find an emerging pattern. After n iterates, the finite geometric series that is the coefficient of $K(x)$ can be written as

$$1 + R_0 + R_0^2 + \cdots + R_0^{n-1} = \frac{R_0^n - 1}{R_0 - 1}. \tag{6.17}$$

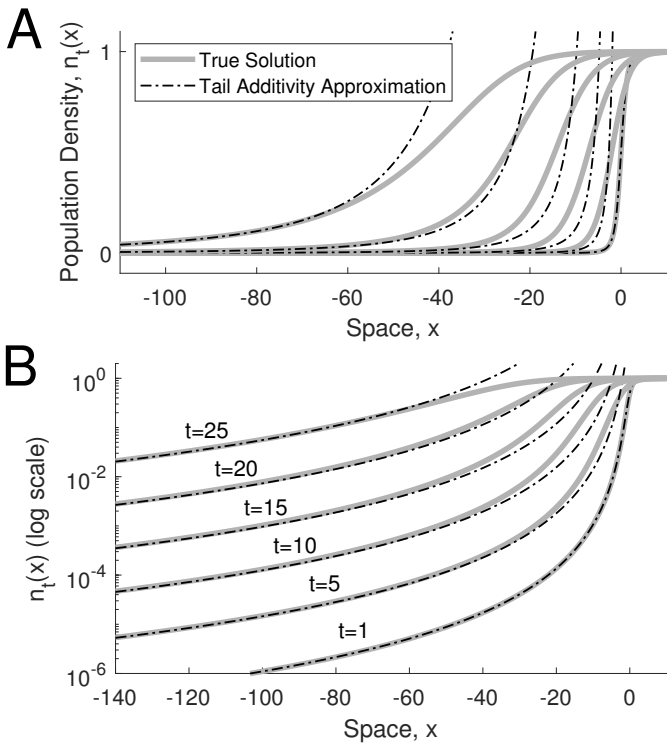

Figure 11: Comparison of true and approximate solution for a front-release invasion. **(A)** The exact solution (gray lines) and the approximation (6.18) due to tail additivity (black dash-dotted lines) plotted at times $t = 1, 5, 10, 15, 20, 25$. The dispersal kernel is the t-distribution ($\nu = 9$) and the growth function is Beverton–Holt with $R_0 = 1.5$. **(B)** The true solution and approximation in log space. The accuracy of the approximation can clearly be seen in the tails.

We ultimately find that

$$n_t(x) \sim \left(\frac{R_0^t - 1}{R_0 - 1}\right) K(x). \tag{6.18}$$

From this we see, similar to approximation (4.6) for point-release invasions, the tail behavior of $n_t(x)$ again mirrors that of the kernel, but now instead of it matching that of the pdf $k(x)$, it matches the cdf $K(x)$.

Figure 11 shows the tail additivity approximation (6.18) for a front-release release invasion with the nonlinear model (2.2) in linear- and log-scales. Similar to the point-release example, the approximation does not appear robust for small x and at linear scale, but when viewed in log-scale the asymptotic convergence of the tails for large x is evident, and can be seen to improve over time.

6.2. Rate of invasion for fat-tailed kernels

For a fat-tailed kernel with degree of tail fatness α, the pdf satisfies $k(x) \sim c(-x)^{-\alpha}$ as $x \to -\infty$, and the cdf will decay at a slower degree of $\alpha - 1$:

$$\begin{aligned} K(x) &= \int_{-\infty}^{x} k(y)\mathrm{d}y \\ &\sim \int_{-\infty}^{x} c(-y)^{-\alpha}\mathrm{d}y \\ &= \tilde{c}(-x)^{-(\alpha-1)}. \end{aligned} \tag{6.19}$$

Thus, the cdf has a fatter tail than the pdf.

To find the invasion rate under such a kernel we proceed in the same way as for point-release invasions; however since we are tracking a leftward-moving invasion we will let $-x_t$ denote the position of the invasion front so that $x_t > 0$. We next set

$$n_{t+1}(-x_{t+1}) = n_t(-x_t) = \overline{N} \tag{6.20}$$

and insert the front-release approximation (6.18) for $n_t(x)$. We obtain

$$(R_0^{t+1} - 1)K(-x_{t+1}) \approx (R_0^t - 1)K(-x_t). \tag{6.21}$$

Assuming that $K(x) \sim \tilde{c}(-x)^{-(\alpha-1)}$, then

$$x_{t+1}^{(\alpha-1)} \approx \left[\frac{R_0^{t+1} - 1}{R_0^t - 1}\right] x_t^{(\alpha-1)}. \tag{6.22}$$

As t increases, the bracketed quantity converges to R_0 (for $R_0 > 1$). As in the case of a point-release we observe geometric growth of the wavefront,

$$x_{t+1} \approx R_0^{1/(\alpha-1)} x_t, \qquad t \to \infty \tag{6.23}$$

however we see that the base of the geometric growth is $R_0^{1/(\alpha-1)}$ for front-release invasions rather than $R_0^{1/\alpha}$ for point-release invasions.

6.3. Other front-release initial conditions

The previous analysis was carried out assuming that the initial condition follows the Heaviside function (6.9). This assumption can be relaxed considerably: the invasion rate will be the same if the initial condition is the cdf of any thin-tailed distribution, or even for any distribution that is less heavy-tailed than the dispersal kernel. This is because if $n_0'(x)$ is a probability density then we can apply the tail additivity theorem (3.29) where one density dominates the other. Therefore

$$\begin{aligned} n_1'(x) &= \int_{-\infty}^{\infty} k(x-y) n_0'(y)\mathrm{d}y \\ &= \big(k * n_0'\big)(x) \\ &\sim k(x), \qquad x \to -\infty. \end{aligned} \tag{6.24}$$

Integrating to re-obtain $n_1(x)$, we have

$$n_1(x) \sim K(x), \tag{6.25}$$

which generalizes (6.10). This means that the initial front-release condition can be, for example, a linear transition from zero to one occurring over any finite width, or a smooth logistic curve.

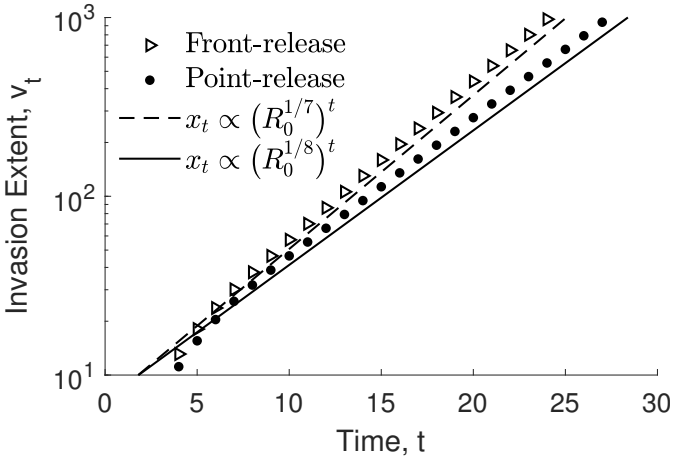

Figure 12: Front-release invasions spread at a faster geometric rate than point-release invasions. The plot show the invasion extent over time for point- and front-release invasions under the nonlinear model with Beverton–Holt growth ($R_0 = 4$) and fat-tailed Laplace-kernel dispersal. In log space, the invasion extents tend to straight line trends that indicate geometric growth. The fact that the two trends diverge shows that the rates of geometric growth differ between point- and front-release invasions. The two lines correspond to the rates predicted by our analyses. The numerical domain has half-width $H = 15\,000$ and grid-spacing $\Delta x = 0.1$.

7. Invasion rates and initial conditions

Our point- and front-release analyses show that the asymptotic invasion rate of a fat-tailed invasion depends on its initial condition. The tail decay of point-release invasions mirrors that of the dispersal kernel pdf $k(x)$, whereas the tail decay of front-release invasions is like that of its cdf $K(x)$. For fat-tailed kernels, the cdf has a slower rate of decay than the pdf; if $k(x)$ has tail fatness of degree α, then $K(x)$ will have degree $\alpha - 1$. This in turn means that point-release invasions will invade geometrically with base $R_0^{1/\alpha}$ and front-release with base $R_0^{1/(\alpha-1)}$.

This shows that the initial condition of a fat-tailed invasion can have a lasting effect on the ultimate invasion rate of the population; the initial condition affects the ultimate rate of spread, and the effect is persistent for all time. Point- and front-release invasions will both asymptotically invade at geometric rates, but these rates differ. Figure 12 compares the invasion rates for point- and front-release invasions under the nonlinear model. We plot the invasion extent x_t in logarithmic scale and see straight-line trends that indicate geometric growth. We see good agreement with the analytic predictions; both invasions spread at geometric rates: the point-release invasion with base $R_0^{1/\alpha}$ and the front-release with base $R_0^{1/(\alpha-1)}$. The difference is clearly visible on a logarithmic scale, where the diverging straight-line trends indicate different bases.

7.1. Plateau initial conditions

Our analyses have focused on point-release and front-release invasions: two extreme cases corresponding to invasions beginning with either a small and highly localized population or a large population spread over a semi-infinite area. A natural question is what occurs for intermediate cases: those populations that are not so well-established as to have semi-infinite support, but that also cannot be thought of as initially localized to a point.

To address this we performed simulations with *plateau initial conditions*, where the initial population is one within an interval and zero outside. Precisely, we set $n_0(x) = 1$ for $-W < x \leq 0$ and $n_0(x) = 0$ elsewhere. We simulated plateaus on domains with half-width $H = 2^N$ and plateau widths $W = 2^0, 2^1, 2^2, \ldots, 2^N$ so as to range from the case of a near-point-release to a near-front-release. Under our definitions, plateau initial conditions are not front-like (they are zero at both positive and negative infinity) but they become locally front-like as their width is increased. Extending the back of the plateau to larger negative values brings the local behavior of the plateaus near the origin into closer agreement with a front-release.

For a population invading at a geometric rate with $x_{t+1} = \rho x_t$, the invasion speed $v_t = x_t - x_{t-1}$ also obeys the relation $v_t = \rho v_{t-1}$. Computing v_t/v_{t-1} reveals the per-step rate of geometric growth. We expect $v_t/v_{t-1} \to R_0^{1/\alpha}$ for a point-release invasion and $v_t/v_{t-1} \to R_0^{1/(\alpha-1)}$ for a front-release. Figure 14 shows plots of the computed speed ratio for plateau initial conditions with t-distribution dispersal. We see that for all plateau widths, the invasion experiences a transient period of around ten to twenty generations as the invasion front is established and the rate of acceleration stabilizes. For narrow

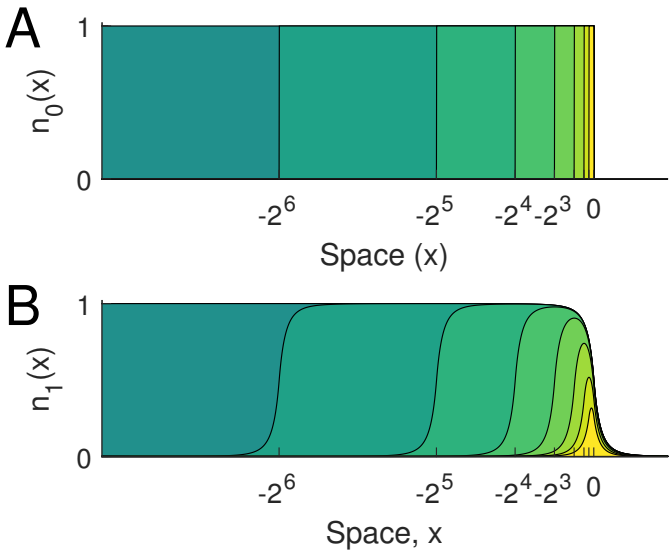

Figure 13: Plateau initial conditions. These conditions are intermediate between a point release and a front-release. **(A)** Each shaded region shows an initial condition $n_0(x)$ that is a "plateau" of width $W = 2^k$ for $k = 0, 1, 2, \ldots, 7$. **(B)** The first generation $n_1(x)$ following a plateau-release. The populations do not interact with one another. For narrow plateaus the generations look like a point release. The population densities line up at the right as the plateau width is increased, and converge to a front release.

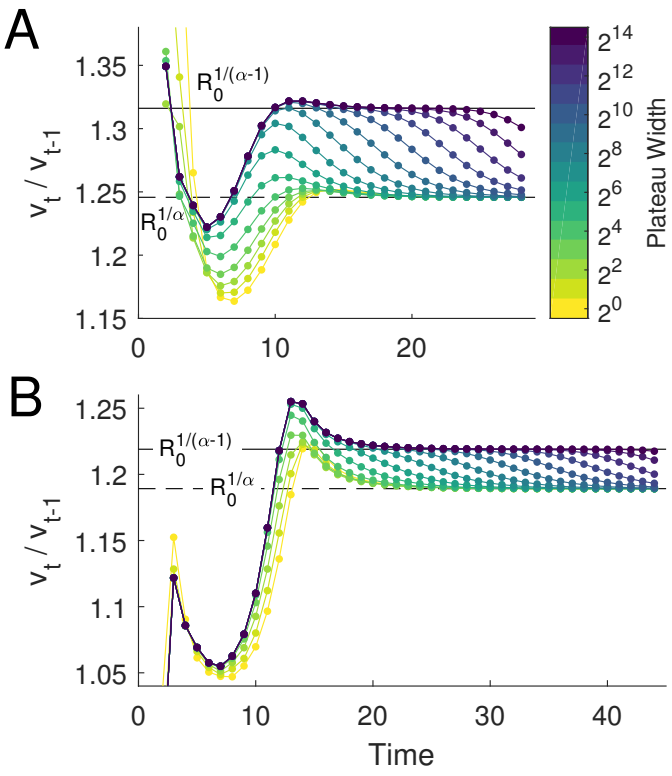

Figure 14: Invasion rates following plateau initial conditions. Plateau initial conditions produce invasions whose behavior shares qualities of both point- and front-release invasions. As the plateau width increases, the initial condition more closely resembles a front-release invasion, and so the invasion initially progresses geometrically with base $R_0^{1/(\alpha-1)}$ as is characteristic of a front-release invasion. After a delay related to the width of the plateau, the invasion slows to the rate associated with point-release invasions: geometric with base $R_0^{1/\alpha}$. **(A)** Plateau invasions with fat-tailed Laplace-kernel dispersal ($\alpha = 5$) and $R_0 = 3$. The grid spacing is $\Delta x = 0.25$ and domain half-width $H = 2^{14}$. **(B)** Plateau invasions with t-distribution dispersal ($\nu = 7$) and $R_0 = 4$. The grid spacing is $\Delta x = 0.5$ and domain half-width $H = 2^{14}$.

plateaus, the speed ratio approaches the predicted rate for point-release invasions, $R_0^{1/\alpha}$. For wide plateaus, the speed ratio instead approaches the predicted rate for front-release invasions, $R_0^{1/(\alpha-1)}$, but eventually declines and approaches $R_0^{1/\alpha}$. This makes intuitive sense because in the short-term a plateau initial condition looks and behaves like a front-release. On the other hand, in the long-term a spreading invasion will eventually dwarf any bounded initial condition, which will by that point more closely resemble a point-release. Only a genuine front-release with unbounded support will not resemble a point-release in the long-term when compared against an ever-expanding invaded territory, and can maintain the greater rate of invasion for all time.

8. Accelerating waves

In this section we outline the major qualitative differences between constant-speed and accelerating invasions

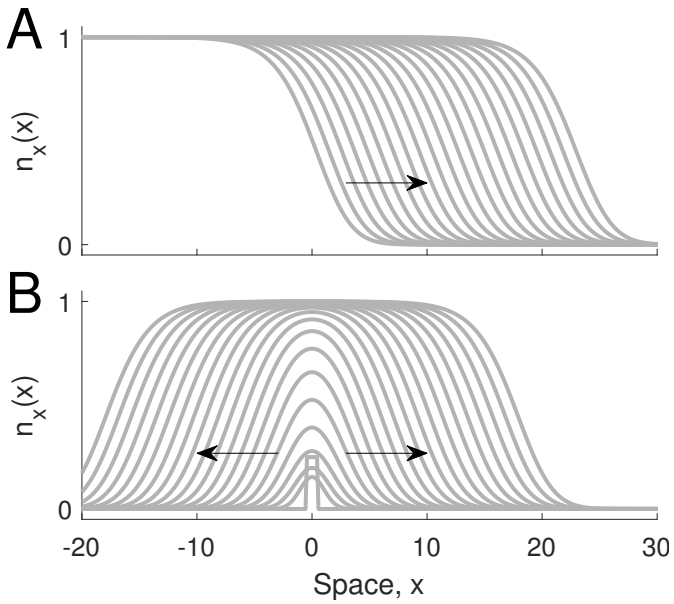

Figure 15: Thin-tailed invasions. Plots show twenty generations of **(A)** a traveling wave solution and **(B)** a point-release invasion. The invasion fronts of the point-release invasion quickly converge to match the shape of the constant-speed traveling waves. Solutions are computed numerically on a domain with half-width $H = 400$, $\Delta x = 1/16$ with Beverton–Holt growth with $R_0 = 2.0$, and Gaussian (standard normal) dispersal).

and what these differences mean in terms of measurement and analysis.

8.1. *Constant-speed invasions*

Traveling waves are a cornerstone of thin-tailed invasions. A traveling wave solution has the form

$$n_t(x) = w(x - ct) = w(z), \tag{8.1}$$

where $z = x - ct$ is the *traveling wave coordinate*, a moving frame of reference that keeps pace with the movement of the wave. Figure 15A shows an example traveling wave generated by Gaussian dispersal with Beverton–Holt growth. The profile of the invasion front is preserved between generations and translates at a consistent rate or speed c so that

$$n_{t+1}(x) = n_t(x - c). \tag{8.2}$$

Any spatial position linked to features of the wave, such as the position of level sets or a point beyond which the wave integrates to a specific value, moves with the wave at the speed c. This means that many measures of invasion are equivalent.

Systems with thin-tailed dispersal often support traveling wave solutions of various speeds and have a minimum wave speed $c_{\min}$. When the initial condition is front-like, the solution will converge to a traveling wave. The wave speed is usually $c_{\min}$ when the initial condition is identically zero in the uninvaded territory or when the initial

population density decays sufficiently rapidly. The traveling wave can be boosted to greater speeds by specifying initial conditions that decay exponentially into the uninvaded territory, and can even be made to accelerate when heavy-tailed initial conditions are given (Alfaro, 2017).

The importance of the theory of traveling waves extends beyond front-release invasions. Even when the initial condition is compactly supported the invasion fronts of a population that successfully invades will mirror those of a traveling wave, as can be seen in Figure 15B. The *spreading speed* c^* is defined as the unique speed that keeps pace with any invasion emanating from compact initial conditions

A significant result states that the minimum wave speed matches the spreading speed: $c^* = c_{\min}$. This is a powerful result that is not immediately obvious. As a consequence, the question of the speed of thin-tailed invasions is greatly simplified: for virtually any initial condition used in practice, the invasion speed will be the same.

8.2. Accelerating invasions

The notion of an invasion front is fundamentally different in accelerating invasions from those with constant speed. In a traveling wave the invasion front has a characteristic width such that the population level is negligible far ahead of the invasion. In an accelerating invasion the front has no fixed width, and actually grows without bound. This means that at successive generations a larger and larger patch surrounding the front has population density comparable to that of the front position. An example of this can be seen in Figure 16, where the length of the domain captured between two level sets grows over time.

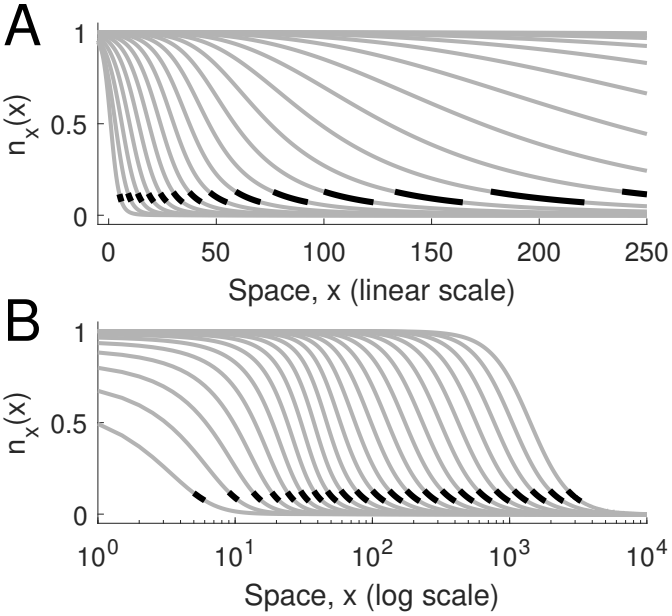

Figure 16: Invasion fronts of a geometrically accelerating invasion plotted using linear and logarithmic scales. Plots show $n_t(x)$ for $t = 5, 10, \ldots, 60$ for a front-release invasion with t-distribution ($\nu = 3$) dispersal. **(A)** The fat-tailed invasion advances at an accelerating rate and the invasion front stretches and elongates as its speed increases. **(B)** Plotting with x on a logarithmic scale the accelerating invasion front converges to a consistent profile akin to a traveling wave. The domain half-width is $H = 10\,000$, $\Delta x = 0.5$, and growth is Beverton–Holt with $R_0 = 1.2$.

The traveling wave coordinate is not useful for analyzing accelerating waves since their shape and speed change with time. Since the invasion extent x_t grows geometrically, it is instead natural to apply a logarithmic transformation to the spatial variable. Figure 16 shows an accelerating invasion plotted in both normal space and log-transformed space. We see that on a linear-linear plot the invasion front elongates whereas in log-linear plot the invasion front tends to a consistent shape, similar to that of a traveling wave.

The fact that point- and front-release invasions have differing rates of spread is another major indication that fat-tailed invasions are fundamentally different from thin-tailed ones and require careful attention. For thin-tailed invasions, the minimum wave speed is equivalent to the spreading speed; this means we need only find one invasion speed, regardless of the initial condition. Our results for point-, front-, and plateau-release invasions demonstrate that there is no equivalence of invasion rate between compact-release and front-release invasions when dispersal is fat-tailed. The rate of spread for fat-tailed invasions has fundamental dependence on the initial condition.

8.3. Rates of invasion

Thin-tailed invasions converge to constant-speed traveling waves, and we say that their rate of spread is linear. A large body of work is in place around this paradigm: approaches for finding the speed and even definitions for the speed are built around the assumption that the speed will approach a constant value. As an example, Kot and Neubert (2008) derived the invasion speed for thin-tailed kernels by taking the limit of distance divided by time,

$$c = \lim_{t\to\infty} \frac{x_t}{t}. \tag{8.3}$$

This and similar definitions take advantage of the fact that in the limit, x_t is proportional to the time t — the bulk of the magnitude of x_t is due to traveling at the speed c, and any transient speedup or slowdown that occurs in finite time is negligible.

The invasion speed can also be calculated on a per-step basis by taking the difference of successive front positions,

$$v_t = x_t - x_{t-1}. \tag{8.4}$$

In the case of thin-tailed invasions, we observe that v_t converges to a finite value, the same speed c found by (8.3).

Accelerating invasions attain ever-greater speeds and so cannot be characterized by a single speed. We therefore draw the distinction that accelerating invasions have invasion *rates* rather than invasion *speeds*. An invasion may

be generally described as having a spread rate, such as polynomial or geometric growth in time. A constant-speed invasion has a *arithmetic* rate of spread that is characterized by a single measurement: the invasion speed, but accelerating invasions necessarily have different rate types. In general each type of invasion rate requires a different characterization.

Geometric growth is characterized by multiplication by a constant growth factor: if the invasion front advances geometrically, then $x_{t+1} = \rho x_t$ for some factor $\rho > 1$. Taking the ratio of the position of the invasion front at successive times will yield the rate of growth between generations. Taking the limit as time becomes large, we recover the asymptotic rate of geometric invasion,

$$\lim_{t\to\infty} \frac{x_{t+1}}{x_t} = \rho. \tag{8.5}$$

The approach of measuring the limiting ratio x_{t+1}/x_t is to our knowledge a new way of measuring the rate of invasion. If misapplied, it can produce misleading or counter-intuitive results. Consider the case of applying (8.5) to a constant-speed invasion where $x_t = ct$: in this case the limiting ratio x_{t+1}/x_t becomes

$$\lim_{t\to\infty} \frac{x_{t+1}}{x_t} = \lim_{t\to\infty} \frac{c(t+1)}{ct} = 1. \tag{8.6}$$

This suggests that asymptotically, $x_{t+1} = x_t$, from which we are tempted to infer that the invasion front is stationary at large times. This faulty reasoning is because a perspective of geometric growth is unsuitable for an invasion progressing at a constant speed: compared to geometric growth, an invasion expanding at a slower rate stands still. Another potential trap is when the rate of geometric growth ρ is made to be one. For any $\rho > 1$, an invasion extent $x_t = \rho^t$ will grow geometrically, even when ρ is very small. When $\rho = 1$ a transition occurs where the behavior is qualitatively different and there is no geometric growth. In our analyses, the net reproductive rate is assumed strictly greater than one, and the behavior in the case $R_0 = 1$ cannot be extrapolated. For this reason we are careful to distinguish between weak and strong Allee effects as well as the degenerate case where $R_0 = 1$ that lies between weak and strong Allee effects.

8.4. Measurements of invasion

The choice to measure the position of the invasion front by a threshold density is intuitive but not the only possibility. Ōkubo (1980) measured the extent of invasion by finding the boundary that separates the bulk of the population from a negligible number of individuals that "have escaped notice by a survey." We call this approach *quantity–exclusion* since the position of the invasion front depends on the exclusion of a fixed number of individuals rather than on population density. These approaches can yield different measures of invasion, as can be seen in Figure 17: in this case, measurement by quantity-exclusion

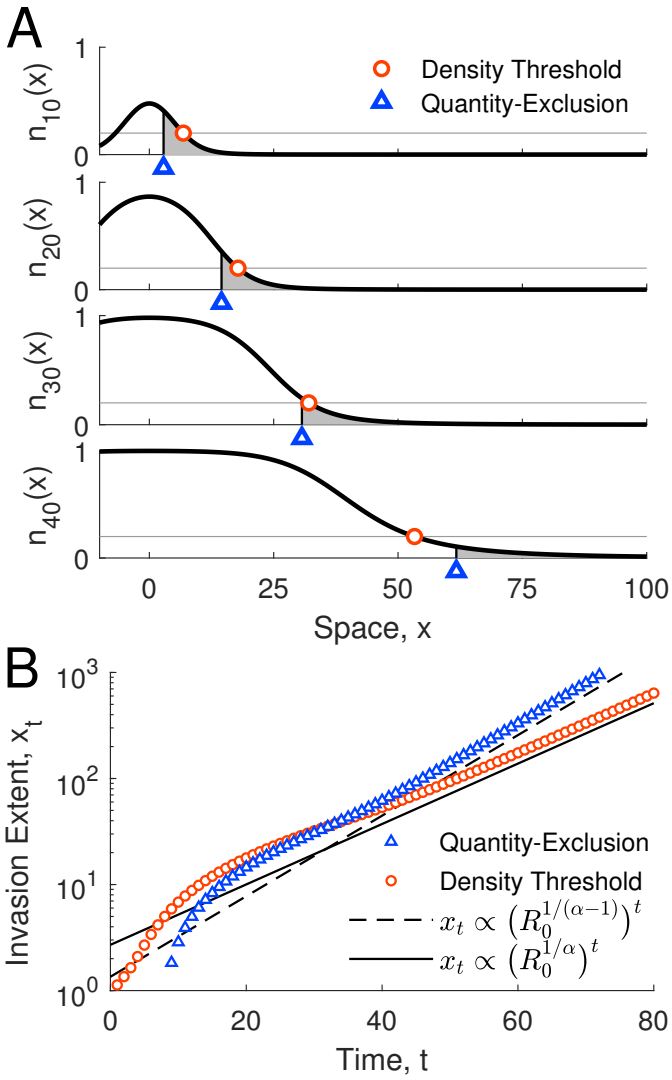

Figure 17: Two approaches for measuring invasion extent. To measure by density-threshold, we set a threshold value $\overline{N}$ and define x_t so that the population density at x_t is $\overline{N}$. To measure by quantity-exclusion we set a fixed quantity of individuals $\overline{Q}$ that lie beyond the invasion extent (area under the curve past x_t). The two measures of extent do not coincide for fat-tailed invasions, and predict different geometric rates of spread. **(A)** A fat-tailed invasion measured by density–threshold and quantity-exclusion at four different times. **(B)** The invasion extent x_t as predicted by the two measurement techniques. The trends diverge in log space, indicating different rates of geometric growth.

is initially behind but eventually overtakes measurement by density-thresholding.

As an example, consider a point-release invasion with fat-tailed dispersal $k(x) \sim cx^{-\alpha}$ under the linear model. Then $n_t(x) \sim cR_0^t t x^{-\alpha}$ as $x \to \infty$ as we found in (4.6).

Integrating the tail of the invasion, we find

$$\begin{aligned}\overline{Q} &= \int_{x_t}^{\infty} n_t(x)\mathrm{d}x \\ &\sim cR_0^t t \int_{x_t}^{\infty} x^{-\alpha}\mathrm{d}x \\ &= \frac{cR_0^t t}{\alpha-1} x_t^{-(\alpha-1)}.\end{aligned} \tag{8.7}$$

Solving for x_t we find

$$x_t \sim \left[\frac{cR_0^t t}{\overline{Q}(\alpha-1)}\right]^{1/(\alpha-1)}. \tag{8.8}$$

Proceeding in the same manner as when we derived the invasion speed for fat-tailed kernels from point-release invasions, we take the ratio x_{t+1}/x_t and obtain

$$\frac{x_{t+1}}{x_t} \approx \left[R_0\left(\frac{t+1}{t}\right)\right]^{1/(\alpha-1)}. \tag{8.9}$$

So in the limit of large time, we see geometric growth at rate $R_0^{1/(\alpha-1)}$,

$$x_{t+1} \approx R_0^{1/(\alpha-1)} x_t, \qquad t \to \infty. \tag{8.10}$$

This differs from our earlier predicted rate of spread (4.12) based on the threshold measure of invasion where the invasion front advanced at a geometric rate of $R_0^{1/\alpha}$. The predicted invasion rate is still geometric, but of a different base. The same discrepancy in the base of the exponent is observed when analyzing front-release invasions: with density-thresholding we found it to be $R_0^{1/(\alpha-1)}$ (equation 6.23), however with quantity-exclusion it is $R_0^{1/(\alpha-2)}$.

9. Discussion

In this paper we have demonstrated a new tool for studying fat-tailed invasions. We analyzed linear and nonlinear integrodifference equations and two types of initial conditions using the properties of regular variation and regularly varying densities. Our analyses apply to populations with no Allee effect and weak Allee effects. We have shown that fat-tailed invasions advance asymptotically at geometric rates that depend on the net reproductive rate and the degree of fatness of the tails of the dispersal kernel.

Regular variation. The theory of regular variation as well as regularly varying densities and their associated tail additivity properties are powerful tools for analyzing fat-tailed invasions. These and related distributions are used in probability to obtain asymptotic approximations of probabilities of rare events, and are also used in many other fields. IDE models are especially well-suited to benefit from these tail approximations: the compounding effect of geometric growth over many generations raises the scale of the tails. The presence of Allee effects generally greatly complicates invasion analyses, but in our case both no-Allee and weak-Allee cases can be addressed at once.

Accelerating invasions. There are significant qualitative differences between constant-speed and accelerating invasions. Many of the existing methods for analyzing constant-speed invasions need to be adapted or reworked to accommodate acceleration, including definitions and ways of measuring invasion front position and of rates of growth of an invasion.

Allee effects. We found that invasion under a weak Allee effect behaves essentially the same as when there is no Allee effect: the ultimate rate of invasion is governed entirely by the degree of tail fatness of the kernel and the net reproductive rate, $R_0 = f'(0)$. So long as $R_0 > 1$, the ultimate rate of invasion is geometric. Weak Allee effects that border on the no-Allee or strong Allee case lead to invasions whose transient dynamics can last for long times.

The case where $R_0 = 1$ is the intermediate case where offspring exactly replace their parents, and is sometimes called a "degenerate" case (Alfaro and Coville, 2017); analyses dealing with weak and strong Allee effects may hold when R_0 takes on values arbitrarily close to one, such as $R_0 = 1.001$, but fail when $R_0 = 1$ exactly. In the related field of integrodifferential equations, the difference between accelerating and constant-speed invasions has been connected to the critical transition where $R_0 = 1$, with fat-tailed dispersal kernels yielding accelerating invasions for R_0 strictly greater than one (Garnier, 2011). Our numerical simulations suggest the same of integrodifference equations: that as R_0 is lowered to one, the ultimate accelerating phase of fat-tailed invasions is delayed for increasingly many generations, with the initial constant speed transient phase resembling a constant-speed invasion. The case where $R_0 = 1$ could be thought of as the accelerating phase being delayed for infinitely many generations.

We have not addressed strong Allee effects where $R_0 < 1$. This is because fat-tailed invasions depend so heavily on individuals dispersed far into the tails. In the case of weak Allee effects ($R_0 > 1$), pioneering individuals at low densities may not thrive like those at high densities, but they survive and manage to produce enough offspring to have a net positive increase in the local population that accumulates over time. In the strong Allee case these individuals always die off. This means that there is no growing accumulation of individuals in the tails. Kot et al. (1996) performed a general analysis with a particular strong Allee effect and found that it limited invasion rates to finite speeds for all kernels, even fat-tailed ones. We speculate that even fat-tailed invasions will in general be tempered by strong Allee effects and will not accelerate but instead attain finite invasion speeds.

Constant speed transients. Fat-tailed invasions can exhibit transient behavior for long times during which the invasion speed is near-constant. This phenomenon is present in the case of no Allee effect as well as weak Allee effects. It is most pronounced when R_0 is greater than one

but small. The cause of this phenomenon is complicated but we believe it is due to an interplay between the tail additivity property (3.27) and the central limit theorem, which we hope to address in a future paper. An ecological interpretation for this phenomenon is that of the lag phase or lag time (Crooks, 2005). Lag times are often observed in the initial establishment of invasion species, and can precede rapid expansion phases (Parker, 2004); however, we note that constant speed transients are not limited to point-release invasions, and can also occur for well-established front-release invasions.

Invasion rate dependence on initial conditions. The difference in invasion rates between newly established and well-established populations is to our knowledge a new result. We have shown that fat-tailed invasions from well-established populations (front-release) will invade at a greater geometric rate than newly-emerging ones (point-release) and that this effect is persistent for all time. Thin-tailed invasions can be forced to invade at speeds greater than their natural spreading speed (Murray, 1989) and even at accelerating rates (Alfaro, 2017) by choice of initial condition, but these cases depend on the initial condition slowly decaying into the uncolonized territory; our point- and front-release initial conditions allow for the initial population to be exactly zero in the uninvaded territory.

In practice, populations never fit our idealized descriptions of point-like and front-like, but our analysis shows a capacity for differing rates of invasion not seen in thin-tailed invasions and our simulations show that intermediate situations (the plateau initial conditions introduced in the section *Invasion rates and initial conditions*) can also exhibit varying invasion rates. With our numerical simulations we have also addressed intermediate cases, plateau initial conditions, that lie between the extremes of point- and front-release initial conditions. We found that these intermediate cases have behavior that blends the predicted behavior of point- and front-releases: they initially behave like a front-release but ultimately spread similarly to a point-release after a (potentially long) time.

Generalizing linear spreading speed. Thin-tailed invasions approach finite invasion speeds. The *spreading speed* c^* has the properties that for any compactly-supported initial condition ($n_0(x) = 0$ outside of a bounded set) (Weinberger, 1982), then for all $\varepsilon > 0$,

$$\lim_{t\to\infty} \sup_{|x|>(c^*+\varepsilon)t} |n_t(x) - 0| = 0 \tag{9.1}$$

$$\lim_{t\to\infty} \sup_{|x|<(c^*-\varepsilon)t} |n_t(x) - 1| = 0. \tag{9.2}$$

These conditions have the physical interpretation that an observer moving at a speed $c^* + \varepsilon$ away from the origin in either direction will eventually completely overtake the invasion, whereas one moving at a speed $c^* - \varepsilon$ will eventually be totally engulfed within the invasion (Weinberger et al., 2002). Central to this definition is the assumption that the asymptotic rate of spread will be constant. If the invasion accelerates then there is no finite spreading speed c^*. For fat-tailed dispersal our analyses show that this acceleration is at a geometric rate. This suggests a modified *geometric spread rate* for these advancing wavefronts may have the properties

$$\lim_{t\to\infty} \sup_{|x|>(c^*+\varepsilon)^t} |n_t(x) - 0| = 0 \tag{9.3}$$

$$\lim_{t\to\infty} \sup_{|x|<(c^*-\varepsilon)^t} |n_t(x) - 1| = 0, \tag{9.4}$$

where the difference is that $(c^*\pm\varepsilon)t$ has been replaced with $(c^* \pm \varepsilon)^t$: the reference frame now moves at a geometric rate. Our point-release analysis indicate that for $n_0(x) = \delta(x)$, then $c^* = R_0^{1/\alpha}$, where α is the degree of tail fatness. On the other hand, for front-release invasions we have found the ultimate rate of invasion is $R_0^{1/(\alpha-1)}$; however, we note that this corresponds to an initial condition with semi-infinite support. This suggests the condition that $n_0(x)$ be zero outside of a bounded set may carry over to this modified spreading rate characterization; indeed, when we explored plateau initial conditions in *Invasion rates and initial conditions* we found that bounded but arbitrarily wide initial conditions all eventually tended to the rate of spread consistent with point-release invasions.

Invasion in two dimensions. In this paper we have focused on invasions in one dimension. We did this to introduce regular variation, because the theory on regularly varying densities is most developed for one-dimensional densities, and to form a basis for studying heavy- and fat-tailed dispersal in more generality and in higher dimensions. Modern dispersal research focuses on two-dimensional dispersal, with the most commonly used kernel forms being two-dimensional (Nathan et al., 2012; Bullock et al., 2017). In a future paper we plan to analyze common dispersal forms in two dimensions and the novel features that arise therein.

Subexponential distributions. The tail additivity property (3.27) is not limited to the class of regularly varying densities, but is in fact part of a broader class of probability distributions. A distribution on the positive half-line with unbounded support is *subexponential* if

$$\overline{K * K}(x) \sim 2\overline{K}(x), \qquad x \to \infty, \tag{9.5}$$

where $\overline{F}(x) = \Pr\{X > x\}$ is the tail function or survivorship function. Subexponential distributions have been studied with the goal of generalizing the useful tail additivity property to as large a class of distributions as possible. The definition as well as much of the theory of subexponential distributions is written in terms of tail functions which are more general from the standpoint of probability theory but less useful in applications that deal with probability densities. Beyond being simply written in terms of distribution functions, it has been shown that there exist

subexponential distributions whose density functions lack the expected tail additivity property (Foss et al., 2011). This means that, despite what we may hope, the work cannot be simply 'translated' from distributions (cdfs) to densities (pdfs). If a sufficiently well-behaved subclass of subexponential distributions can be isolated for which tail additivity of the pdf holds, then our results may easily generalize, potentially broadening the scope of these analyses from fat-tailed to more general heavy-tailed kernels. We also note that our analyses for front-release invasions may already generalize, if care is taken to keep all intermediate steps restricted to distribution functions or tail functions.

Alfaro, M., 2017. Slowing Allee effect versus accelerating heavy tails in monostable reaction diffusion equations. Nonlinearity 30, 687–702.

Alfaro, M., Coville, J., 2017. Propagation phenomena in monostable integro-differential equations: acceleration or not? Journal of Differential Equations 263, 5727–5758.

Bateman, A. J., 1950. Is gene dispersion normal? Heredity 4, 353–363.

Beverton, R. J. H., Holt, S. J., 1957. On the dynamics of exploited fish populations. Fisheries Investigations 19.

Bingham, N. H., Goldie, C. M., Omey, E., 2006. Regularly varying probability densities. Publications de l'Institut Mathématique. Nouvelle Série 80(94), 47–57.

Bingham, N. H., Goldie, C. M., Teugels, J. L., 1987. Regular Variation. Cambridge University Press, Cambridge, UK.

Bracewell, R. N., 1986. The Fourier Transform and Its Applications. McGraw Hill, New York.

Britton, N. F., 1986. Reaction-Diffusion Equations and Their Applications to Biology. Academic Press, London.

Bullock, J. M., Clarke, R. T., 2000. Long distance seed dispersal by wind: measuring and modelling the tail of the curve. Oecologia 124, 506–521.

Bullock, J. M., Mallada González, L., Tamme, R., Götzenberger, L., White, S. M., Pärtel, M., Hooftman, D. A. P., 2017. A synthesis of empirical plant dispersal kernels. Journal of Ecology 105, 6–19.

Cain, M. L., Milligan, B. G., Strand, A. E., 2000. Long-distance seed dispersal in plant populations. American Journal of Botany 87, 1217–1227.

Clark, J. S., Silman, M., Kern, R., Macklin, E., HilleRisLambers, J., 1999. Seed dispersal near and far: patterns across temperate and tropical forests. Ecology 80, 1475–1494.

Cooke, R. M., Nieboer, D., Misiewicz, J., 2014. Fat-Tailed Distributions: Data, Diagnostics and Dependence. John Wiley & Sons, Hoboken.

Crooks, J. A., 2005. Lag times and exotic species: the ecology and management of biological invasions in slow-motion. Ecoscience 12, 316–329.

Feller, W., 1971. An Introduction to Probability Theory and its Applications. Vol. 2. John Wiley & Sons, New York.

Fisher, R. A., 1937. The wave of advance of advantageous genes. Annals of Eugenics 7, 355–369.

Foss, S., Korshunov, D., Zachary, S., 2011. An Introduction to Heavy-Tailed and Subexponential Distributions. Springer, New York.

Garnier, J., 2011. Accelerating solutions in integro-differential equations. SIAM Journal on Mathematical Analysis 43, 1955–1974.

Klein, E. K., Lavigne, C., Gouyon, P.-H., 2006. Mixing of propagules from discrete sources at long distance: comparing a dispersal tail to an exponential. BMC Ecology 6, 3.

Kot, M., 1992. Discrete-time travelling waves: ecological examples. Journal of Mathematical Biology 30, 413–436.

Kot, M., Lewis, M. A., Neubert, M. G., 2012. Integrodifference equations. In: Hastings, A., Gross, L. (Eds.), Encyclopedia of Theoretical Ecology. University of California Press, Berkeley, pp. 381–384.

Kot, M., Lewis, M. A., van den Driessche, P., 1996. Dispersal data and the spread of invading organisms. Ecology 77, 2027–2042.

Kot, M., Neubert, M. G., 2008. Saddle-point approximations, integrodifference equations, and invasions. Bulletin of Mathematical Biology 70, 1790–1826.

Kotz, S., Kozubowski, T., Podgorski, K., 2001. The Laplace Distribution and Generalizations: A Revisit with Applications to Communications, Economics, Engineering, and Finance. Birkhäuser, Boston.

Lewis, M. A., 1997. Variability, patchiness, and jump dispersal in the spread of an invading population. In: Tilman, D., Kareiva, P. M. (Eds.), Spatial Ecology: The Role of Space in Population Dynamics and Interspecific Interactions. Princeton University Press, Princeton, New Jersey, pp. 46–69.

Lewis, M. A., Neubert, M. G., Caswell, H., Clark, J. S., Shea, K., 2006. A guide to calculating discrete-time invasion rates from data. In: Cadotte, M. W., McMahon, S. M., Fukami, T. (Eds.), Conceptual Ecology and Invasion Biology: Reciprocal Approaches to Nature. Springer, Dordrecht, Netherlands.

Lewis, M. A., Petrovskii, S. V., Potts, J. R., 2016. The Mathematics Behind Biological Invasions. Springer Berlin Heidelberg, Cham.

Lutscher, F., Seo, G., Aug. 2011. The effect of temporal variability on persistence conditions in rivers. Journal of Theoretical Biology 283 (1), 53–59.

Miller, J., Thomas, J., 1972. Detectors for discrete-time signals in non-Gaussian noise. IEEE Transactions on Information Theory 18, 241–250.

Mollison, D., 1991. Dependence of epidemic and population velocities on basic parameters. Mathematical Biosciences 107, 255–287.

Mundt, C. C., Sackett, K. E., Wallace, L. D., Cowger, C., Dudley, J. P., 2009. Long-distance dispersal and accelerating waves of disease: empirical relationships. American Naturalist 173, 456–466.

Murray, J. D., 1989. Mathematical Biology. Springer-Verlag, Berlin.

Nathan, R., 2005. Long-distance dispersal research: building a network of yellow brick roads. Diversity and Distributions 11, 125–130.

Nathan, R., Etienne Klein, Juan J. Robledo-Arnuncio, Revilla, E., 2012. Dispersal kernels: review. In: Clobert, J., Baguette, M., Benton, T., J.M. Bullock (Eds.), Dispersal Ecology and Evolution. Oxford University Press, Oxford, UK, pp. 187–210.

Nathan, R., Perry, G., Cronin, J. T., Strand, A. E., Cain, M. L., 2003. Methods for estimating long-distance dispersal. Oikos 103, 261–273.

Nathan, R., Schurr, F. M., Spiegel, O., Steinitz, O., Trakhtenbrot, A., Tsoar, A., 2008. Mechanisms of long-distance seed dispersal. Trends in Ecology & Evolution 23, 638–647.

Ōkubo, A., 1980. Diffusion and Ecological Problems: Mathematical Models. Springer-Verlag, Berlin.

Parker, I. M., 2004. Mating patterns and rates of biological invasion. Proceedings of the National Academy of Sciences of the United States of America 101, 13695–13696.

Phillips, A., Kot, M., 2015. Persistence in a two-dimensional moving-habitat model. Bulletin of Mathematical Biology 77, 2125–2159.

Sullivan, L. L., Li, B., Miller, T. E. X., Neubert, M. G., Shaw, A. K., 2017. Density dependence in demography and dispersal generates fluctuating invasion speeds. Proceedings of the National Academy of Sciences 114, 5053–5058.

van den Bosch, F., Metz, J. A. J., Diekmann, O., 1990. The velocity of spatial population expansion. Journal of Mathematical Biology 28, 529–565.

Vasilyeva, O., Lutscher, F., Dec. 2012. How Flow Speed Alters Competitive Outcome in Advective Environments. Bulletin of Mathematical Biology 74 (12), 2935–2958.
URL https://doi.org/10.1007/s11538-012-9792-3

Wang, M.-H., Kot, M., Neubert, M. G., 2002. Integrodifference equations, Allee effects, and invasions. Journal of Mathematical Biology 44, 150–168.

Weinberger, H., 1982. Long-time behavior of a class of biological models. SIAM Journal on Mathematical Analysis 13, 353–396.

Weinberger, H. F., Lewis, M. A., Li, B., 2002. Analysis of linear determinacy for spread in cooperative models. Journal of Mathe-

matical Biology 45, 183–218.

Appendix A. Nonlinear point release

In this appendix we show that for a point-release invasion under the nonlinear model the rate of invasion is geometric with base $R_0^{1/\alpha}$, which matches the linear model. Denoting this rate as ρ, we aim to prove that $\rho = R_0^{1/\alpha}$ by proving that $\rho \geq R_0^{1/\alpha}$ (the lower bound) and $\rho \leq R_0^{1/\alpha}$ (the upper bound).

Lower bound on invasion rate: $\rho \geq R_0^{1/\alpha}$.

We assume that the total population size does not shrink below some fixed number A, so that $A_t \geq A$ for all time. Then from (4.19) we have

$$\begin{aligned} s_t &\geq A + R_0 A + R_0^2 A + \cdots + R_0^{t-1} A \\ &= A\left(\frac{R_0^t - 1}{R_0 - 1}\right). \end{aligned} \tag{A.1}$$

Using this as an underestimate for s_t, we equate $\overline{N} = n_{t+1}(x_{t+1}) = n_t(x_t)$ and use $k(x) \sim cx^{-\alpha}$ to obtain

$$A\frac{R_0^{t+1} - 1}{R_0 - 1} c x_{t+1}^{-\alpha} \approx A\frac{R_0^t - 1}{R_0 - 1} c x_t^{-\alpha}. \tag{A.2}$$

So

$$\left(\frac{x_{t+1}}{x_t}\right)^{\alpha} \approx \frac{R_0^{t+1} - 1}{R_0^t - 1}, \tag{A.3}$$

and in the limit of large time,

$$x_{t+1} \approx R_0^{1/\alpha} x_t. \tag{A.4}$$

This gives the lower bound $\rho \geq R_0^{1/\alpha}$.

Upper bound on invasion rate: $\rho \leq R_0^{1/\alpha}$.

To bound the invasion rate from above, we first establish the following lemma that bounds the invasion rate in terms of a geometric bound on the total offspring A_t.

Lemma 1. *Assume that $A_t < c\gamma^t$ for some $c > 0$ and $\gamma > 1$. Then the rate of geometric invasion of the nonlinear model is bounded above by geometric growth with base $\max\left\{R_0^{1/\alpha}, \gamma^{1/\alpha}\right\}$.*

Proof. Using the upper bound on A_t and the full form (4.19) of s_t, we have

$$\begin{aligned} s_t &\leq R_0^0 c\gamma^{t-1} + R_0^1 c\gamma^{t-2} + \cdots + R_0^{t-1} c\gamma^0 \\ &= \frac{R_0^t - \gamma^t}{R_0 - \gamma}. \end{aligned} \tag{A.5}$$

Again using this as an underestimate for s_t, we set $\overline{N} = n_{t+1}(x_{t+1}) = n_t(x_t)$ and using $k(x) \sim cx^{-\alpha}$, we have

$$\frac{R_0^{t+1} - \gamma^{t+1}}{R_0 - \gamma} c x_{t+1}^{-\alpha} \approx \frac{R_0^t - \gamma^t}{R_0 - \gamma} c x_t^{-\alpha}. \tag{A.6}$$

Then

$$\left(\frac{x_{t+1}}{x_t}\right)^{\alpha} = \frac{R_0^{t+1} - \gamma^{t+1}}{R_0^t - \gamma^t}. \tag{A.7}$$

If $R_0 > \gamma$, then this the right-hand side tends to R_0, whereas if $\gamma > R_0$, then it tends to γ. Thus

$$x_{t+1} \approx \max\left\{R_0^{1/\alpha}, \gamma^{1/\alpha}\right\} x_t. \tag{A.8}$$

□

Denote R_m as the maximal rate of reproduction,

$$R_m = \inf\left\{R : Rn \geq f(n), \forall n > 0\right\}. \tag{A.9}$$

This value corresponds to the least net reproductive rate among all linear growth functions that over-approximate $f(n)$. For a smooth growth function $f(n)$, the line $R_m n$ is the most shallow tangent line that lies above $f(n)$ for all $n \geq 0$.

The linear model with net reproductive rate R_m bounds the nonlinear model from above, and so also bounds its rate of spread. The rate of spread for the linear model is $R_m^{1/\alpha}$ from our analysis of the linear model, and so we obtain the bound

$$\rho \leq R_m^{1/\alpha}. \tag{A.10}$$

A bound on the rate of spread (position of the invasion front x_t) can in turn be used to bound the rate of growth of the entire population size with the following lemma,

Lemma 2. *If $n_t(x) \sim Ax^{-\alpha}$, then the total population is*

Proof. If $n_t(x) \sim Ax^{-\alpha}$, then the position x_t at which the invasion front falls below an arbitrarily small threshold value ε satisfies $n_t(x_t) = \varepsilon$, then

$$x_t \approx \left(\frac{A}{\varepsilon}\right)^{1/\alpha}. \tag{A.11}$$

The total population P_{tail} in the tail beyond the position x_t can be found by

$$\begin{aligned} P_{\text{tail}} &= \int_{x_t}^{\infty} n_t(x)\mathrm{d}x \\ &\sim \int_{x_t}^{\infty} Ax^{-\alpha}\mathrm{d}x \\ &= \frac{A}{\alpha - 1}\left[x^{-(\alpha-1)}\right]_{\infty}^{x_t} \\ &= \frac{A}{\alpha - 1} x_t^{-(\alpha-1)} \\ &\approx \left(\frac{A}{\alpha - 1}\right)\left(\frac{A}{\varepsilon}\right)^{-1+1/\alpha} \\ &= \frac{A^{1/\alpha}\varepsilon^{1-1/\alpha}}{\alpha - 1} \end{aligned}$$

□

Using this rate of spread as an upper bound we obtain a geometric bound on the total population N_t at each iteration: $N_t < c\gamma^t$ with $\gamma = R_m^{1/\alpha}$. Since $k(x)$ is a redistribution kernel, the number of offspring A_{t-1} equals the total population of the next generation N_t, so $A_{t-1} = N_t$. We therefore obtain a geometric bound on the total offspring, $A_t < c\gamma^t$ with $\gamma = R_m^{1/\alpha}$. Using the previous lemma we have that the rate of spread is the maximum of $R_0^{1/\alpha}$ and $\gamma^{1/\alpha} = R_m^{1/\alpha^2}$, so

$$\rho \leq \max\left\{R_0^{1/\alpha}, R_m^{1/\alpha^2}\right\}. \tag{A.12}$$

If $R_m^{1/\alpha^2} < R_0^{1/\alpha}$, we have achieved the desired goal of bounding ρ. Otherwise, let $\gamma = R_m^{1/\alpha^2}$ and repeat the argument, to obtain

$$\rho \leq \max\left\{R_0^{1/\alpha}, R_m^{1/\alpha^3}\right\}. \tag{A.13}$$

This process can be continued until we obtain $R_m^{1/\alpha^k} < R_0^{1/\alpha}$ for some integer $k > 0$. At this point the tightened the upper bound to obtain

$$\rho \leq R_0^{1/\alpha}, \tag{A.14}$$

as desired.